A Hybrid Model Predictive Control Framework for Docking & Stabilization of Composite Rigid Spacecraft Dynamics

Himadri Basu*, Piyush P. Jirwankar†, Ricardo G. Sanfelice‡
University of California Santa Cruz, Santa Cruz, CA 95060, USA

Miguel Castroviejo-Fernandez§, and Ilya Kolmanovsky¶
University of Michigan, Ann Arbor, MI 48109-2140, USA

This paper presents a hybrid model predictive control (MPC)–based framework for the rendezvous and docking of a deputy spacecraft and a passively tumbling chief on a circular orbit. Both spacecraft are modeled as rigid bodies with coupled translational and rotational dynamics. The objective is to safely guide the deputy spacecraft to dock with the chief spacecraft, and stabilize the motion of the composite rigid body. Depending on the proximity between these spacecraft, the overall control problem is partitioned into two phases—1) capture, and 2) post-capture phase—each with unique control objectives, dynamical models, and constraints. During the capture phase, unanticipated low velocity collision contacts between the spacecraft are taken into consideration, while in the post-capture phase, simultaneous stabilization of the tumbling motion and guiding the composite system to a predetermined parking orbit are achieved. Simulation results are reported to demonstrate the effectiveness of the proposed control framework.

I. Introduction

Autonomous guidance, navigation, rendezvous and proximity operations (RPO) are essential in space missions involving satellite servicing, repairing and refueling, in-space assembly, and towing [1]. In such operations, a controlled spacecraft, commonly referred to as the deputy, is required to recover a chief satellite that is otherwise passively tumbling [2]. To achieve this goal in dynamic space environment under stringent constraints, model predictive control (MPC) is a natural choice as it optimizes a performance index over a receding horizon while explicitly enforcing state and input constraints [3, 4] under uncertainty. RPO missions, however, typically proceed through distinct phases with differing objectives, constraints, dynamics, and available measurements. Accordingly, the closed-loop system is often modeled as a multimode system, where each phase is assigned a controller tailored to its requirements, while a supervisory logic coordinates switching between these controllers to ensure robust performance and prevent chattering [5, 6].

In this paper, we propose a hybrid MPC framework for an RPO mission. The control objectives are to (i) synchronize the deputy's motion with the chief's and achieve soft docking while maintaining continuous line-of-sight to the docking port, and, once docked, (ii) stabilize the composite spacecraft and transfer it to a parking orbit. During the pre-docking phase, we explicitly account for inadvertent low-velocity, non-resting contacts that may arise from unanticipated interactions between the vehicles, while in the docked phase we model sudden decoupling events that transition the dynamics from a composite body back to two separate rigid spacecraft. Due to varied objectives, constraints, and the computational challenges associated with formulating the overall control goal into one complex optimization framework, the problem is divided into two modular control subproblems, one for the capture phase, and the other one for post capture phase. A proximity-based supervisory logic then switches between these controllers as the system approaches or departs from the docking configuration, selecting the appropriate optimization problem to generate control commands.

In contrast to the typical point-mass model assumptions in [3, 4, 7–9], in this paper, we treat the deputy and chief spacecraft as rigid bodies and account for their translational and rotational relative motion dynamics. Unlike [10–12], where the relative orbit and attitude control have been treated separately, the relative motion model considered in this work, inspired by [13], employs a nonlinear coupled translational and rotational dynamics. To reduce the computational

*Postdoctoral Researcher, Department of Electrical and Computer Engineering
†PhD Student, Department of Electrical and Computer Engineering
‡Professor, Department of Electrical and Computer Engineering
§PhD Student, Department of Aerospace Engineering
¶Professor, Department of Aerospace Engineering, AIAA Associate Fellow

complexity of these subproblems, local linearization of the nonlinear equations of motion is performed around the docking configuration for the capture phase, and around the chief's initial target orbit for the post-capture phase. Furthermore, unlike much of the existing literature, we do not assume the docking port is inertially fixed or rotates at a constant angular velocity. Instead, we allow time-varying chief motion, provided the chief's attitude and angular velocity in the chosen reference frame can be accurately estimated or predicted.

Additionally, we explicitly account for the low-velocity collision contacts between the rigid bodies during the capture phase, and sudden decoupling from the composite system in post-capture phase. As noted in [1, 14], inadvertent collisions due to the velocity residuals might be caused by unmodeled perturbations, sensor malfunctions, and computational delays in generating accurate control commands [15–17]. We developed a rigid body contact and collision response models in [18], and a hybrid MPC solution that dynamically updates its objective function upon collisions, assigning higher penalties to misalignment and asynchronization than to proximity. This collision-aware adaptation mechanism mitigates the risk of future collisions, and ultimately ensure a successful docking process. During the post-capture phase, while the composite body is tracking its orbit, internal spring–damper transients at the docking interface may trigger a snap or separation event [19], causing the system to break into two rigid bodies as in the capture phase. Accordingly, the coupling and decoupling dynamics in the post-capture phase, analogous to the inadvertent collision contacts during capture, are modeled within a hybrid-system framework [20]. With a hybrid model that captures the system dynamics for each mode, we formulate different MPC optimization problems to compute the control inputs subject to the objectives and constraints specific to that mode. This hybrid MPC framework is augmented with a discrete supervisory logic with hysteresis, as in [21], to govern mode transitions and ensure robustness across switching surfaces.

Our contributions are summarized as follows. We consider (I) a nonlinear rigid body relative motion model which accounts for the coupled translational and rotational relative motion dynamics of the chief and deputy spacecraft; (II) we treat multi-body stabilization and trajectory tracking problems in both capture and post-capture phases; (III) unanticipated rigid-body contacts and decoupling of the docked pair has been explicitly accounted for; (IV) we propose a unified hybrid MPC formulation which exploits switching logic to systematically integrate the control designs in the two phases; and finally, (V) we verify the effectiveness of our proposed approach in numerical simulations. Additional details (derivation of the linearized state space dynamics in Section V) are omitted here and will be addressed in a forthcoming publication.

Notation: Let $\mathbb{R}^n$ denote the $n-$dimensional Euclidean space. Additionally, let $\mathbb{R}_{\geq 0}$ denote the set of nonnegative real numbers, and $\mathbb{N}$ the set of nonnegative integers. Given vectors $x, y \in \mathbb{R}^n$, $(x, y) \coloneqq [\, x^\top \; y^\top \,]^\top$, and for any two matrices A and B of identical column dimensions, $(A, B) \coloneqq [\, A^\top \; B^\top \,]^\top$. Given square matrices A and B, $\mathrm{diag}(A, B)$ denotes a block diagonal matrix with diagonal terms being A and B. Let $\mathbf{1}_n$ denote the $n-$dimensional vector of all ones and $\mathbf{0}$ represent a zero matrix, with its dimension inferred from context. The Kronecker product of matrices is given by the symbol $\otimes$. The function $\Psi_1 : \mathbb{R}^n \times \mathbb{R}^m \to \mathbb{R}^n$ is introduced as the standard projection onto $\mathbb{R}^n$ such that $\Psi_1(x, y) = x$, and similarly, let $\Psi_2 : \mathbb{R}^n \times \mathbb{R}^m \to \mathbb{R}^m$ be such that $\Psi_2(x, y) = y$. Given a vector x and a matrix M, the symbols $|x|$ and $|M|$ represent the Euclidean norm and the induced matrix 2-norm, respectively. Given two symmetric matrices $A, B \in \mathbb{R}^{n\times n}$, the symbol $A \succ B$ indicates that the matrix $A - B$ is positive definite (a symmetric matrix with strictly positive real eigenvalues). For $x = (x_1, x_2, x_3) \in \mathbb{R}^3$, the skew-symmetric matrix $x^\times$ is given by

$$x^\times \coloneqq \begin{bmatrix} 0 & -x_3 & x_2 \\ x_3 & 0 & -x_1 \\ -x_2 & x_1 & 0 \end{bmatrix} \in \mathbb{R}^{3\times 3}. \tag{1}$$

Given an angle $\theta \in \mathbb{R}$ and an axis of rotation (unit vector) $\hat{n} \in \mathbb{R}^3$, a rotation matrix $\mathcal{R} : \mathbb{R} \times \mathbb{R}^3 \to SO(3)$ can be parametrized by the Rodriguez formula [22] as

$$\mathcal{R}(\theta, \hat{n}) = I + \sin(\theta)\, \hat{n}^\times + \big(1 - \cos(\theta)\big)\, \hat{n}^\times \hat{n}^\times \tag{2}$$

where $SO(3) = \big\{\mathcal{R} \in \mathbb{R}^{3\times 3} : \mathcal{R}^\top \mathcal{R} = I,\ \det \mathcal{R} = 1\big\}$ is a special orthogonal group of order three. Let $\mathbb{Q}_u$ represent the set of unit quaternions, defined as $\mathbb{Q}_u \coloneqq \{q = (q_\eta, q_\mu) : q_\eta \in \mathbb{R}^3, q_\mu \in \mathbb{R}, |q| = 1\}$. In terms of the rotation axis $\hat{n} \in \mathbb{R}^3$ and the rotation angle $\theta \in \mathbb{R}$, a unit quaternion can also be parameterized as

$$q = \begin{pmatrix} \underbrace{\sin\left(\frac{\theta}{2}\right)\hat{n}}_{q_\eta}, & \underbrace{\cos\left(\frac{\theta}{2}\right)}_{q_\mu} \end{pmatrix}, \tag{3}$$

with the direction cosine matrix associated with q being given as

$$\mathcal{R}(q) \coloneqq \left(q_\mu^2 - q_\eta^\top q_\eta\right) I_3 + 2q_\eta q_\eta^\top - 2q_\mu q_\eta^\times. \tag{4}$$

If $\theta = 2k\pi$, for any $k \in \mathbb{N}$, $q \coloneqq (\mathbf{0}, 1)$, corresponding to the identity rotation matrix $\mathcal{R}(q) = I_3$. Furthermore, for a rotation matrix $\mathcal{R}$, from (4), $\log(\mathcal{R}) = \theta(\mathcal{R} - \mathcal{R}^\top)/2\sin\theta = \theta\hat{n}^\times = 2\arctan\left(|q_\eta|/q_\mu\right) q_\eta/|q_\eta|$. For convenience, we use $q_I \coloneqq (\mathbf{0}, 1) \in \mathbb{Q}_u$ to denote the identity quaternion. Given a vector $\mathbf{x}$, we use the symbol $\mathbf{x}_{|\mathcal{I}}$, when expressed in a coordinate frame $\mathcal{I}$. Given a set $\mathcal{A}$, the symbol $\overline{\mathcal{A}}$ denotes its closure. Given a vector $x \in \mathbb{R}^n$ and a closed set $A \subset \mathbb{R}^n$, the distance from x to A is defined as $|x|_A = \inf_{z\in A}|x - z|$.

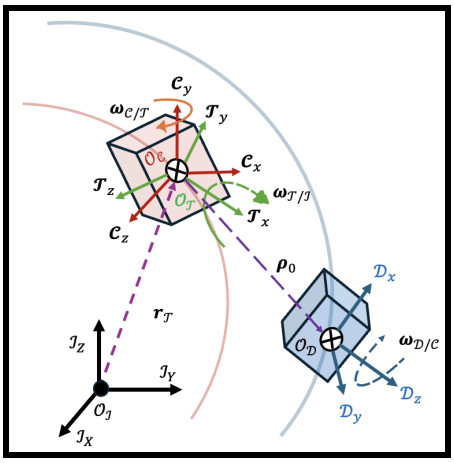

(a) Coordinate frames.

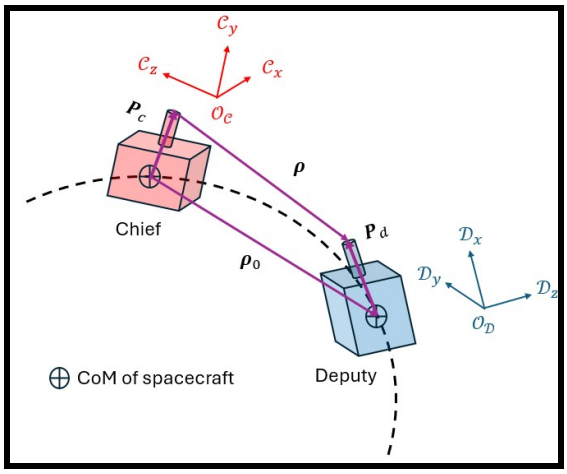

(b) Orientation of the rigid bodies and displacement between docking ports.

Fig. 1 Coordinate frames for rigid body relation motion in proximity operations.

II. Preliminaries

A. Coordinate Frames

In this paper, we consider the mission involving autonomous docking of a deputy spacecraft to a passively tumbling uncooperative chief spacecraft in a circular low Earth orbit, followed by stabilizing the motion of the docked assembly and transfering it to a parking orbit. The coordinate frames used to describe the relative motion and orientation between the chief and deputy spacecraft are defined in Figure 1.

- Earth-centered inertial (ECI) frame $\mathcal{I} \coloneqq \{O_\mathcal{J}, \mathcal{J}_X, \mathcal{J}_Y, \mathcal{J}_Z\}$ with its origin $O_\mathcal{J}$ located at the center of mass (CoM) of Earth, X axis pointing towards the vernal equinox, Z axis towards the north pole, and Y axis pointing eastward completing the right-handed triad.
- Local-vertical-local-horizontal (LVLH) frame $\mathcal{T} \coloneqq \{O_\mathcal{T}, \mathcal{T}_x, \mathcal{T}_y, \mathcal{T}_z\}$ which is a rotating frame with its origin located at the CoM of the chief spacecraft, $\mathcal{T}_x$ axis (LV) pointing radially outward from the CoM of Earth to the CoM of the chief spacecraft, $\mathcal{T}_y$ axis (LH) towards the chief spacecraft's instantaneous velocity vector in the orbital plane, and $\mathcal{T}_z$ axis pointing along the angular momentum vector.
- Body frames $C \coloneqq \{O_C, C_x, C_y, C_z\}$ and $\mathcal{D} \coloneqq \{O_\mathcal{D}, \mathcal{D}_x, \mathcal{D}_y, \mathcal{D}_z\}$ are rotating coordinate frames with their origins at the centers of mass of the chief and deputy spacecraft, respectively, and their axes are aligned with each spacecraft's principal axes of inertia.

Let the displacement between CoMs of frame $\mathcal{T}$ and ECI frame $\mathcal{I}$ be denoted as $\boldsymbol{r}_\mathcal{T}$, between C and $\mathcal{D}$ by $\boldsymbol{\rho}_0$, and between the docking ports by $\boldsymbol{\rho}$. Let $\boldsymbol{P}_c$ be the position vector from the CoM of the chief spacecraft (mass m_c) to its docking port and let $\boldsymbol{P}_d$ be the position vector from the CoM of the deputy spacecraft (mass m_d) to its docking port. Let the angular velocities of the frame $\mathcal{T}$ relative to $\mathcal{I}$, C relative to $\mathcal{T}$, and $\mathcal{D}$ relative to C be denoted as $\boldsymbol{\omega}_{\mathcal{T}/\mathcal{I}}$, $\boldsymbol{\omega}_{C/\mathcal{T}}$, and $\boldsymbol{\omega}_{\mathcal{D}/C}$, respectively. Let $\boldsymbol{\rho}_n$ denote the position vector of COM of the composite chief-deputy spacecraft in frame $\mathcal{T}$,

and $\dot{\boldsymbol{\rho}}_n$ denote the velocity. Let $\boldsymbol{F}_d$, and $\boldsymbol{M}_d$ denote the control thrust and torque vectors acting on the deputy spacecraft, respectively. With these definitions, we now introduce the following quantities:

$$\begin{aligned} \omega_c &\coloneqq \boldsymbol{\omega}_{\mathcal{C}/\mathcal{T}|\mathcal{C}}, \quad \omega \coloneqq \boldsymbol{\omega}_{\mathcal{D}/\mathcal{C}|\mathcal{D}}, \quad \omega_t \coloneqq \boldsymbol{\omega}_{\mathcal{T}/\mathcal{I}|\mathcal{T}}, \quad \omega_d \coloneqq \boldsymbol{\omega}_{\mathcal{D}/\mathcal{T}|\mathcal{D}}, \quad M_d \coloneqq \boldsymbol{M}_d|_{\mathcal{D}}, \\ \rho_0 &\coloneqq \boldsymbol{\rho}_0|_{\mathcal{T}}, \quad \rho \coloneqq \boldsymbol{\rho}_{|\mathcal{C}}, \quad P_c \coloneqq \boldsymbol{P}_{c|\mathcal{C}}, \quad P_d \coloneqq \boldsymbol{P}_{d|\mathcal{D}}, \quad \rho_n \coloneqq \boldsymbol{\rho}_n|_{\mathcal{T}}, \quad F_d \coloneqq \boldsymbol{F}_d|_{\mathcal{D}}. \end{aligned} \tag{5}$$

Let the orientation of $\mathcal{D}$ relative to $\mathcal{C}$, and $\mathcal{C}$ relative to $\mathcal{T}$, be parameterized by unit quaternions $q \in \mathbb{Q}_u$ and $p \in \mathbb{Q}_u$, respectively, with corresponding direction cosine matrices $Q \coloneqq \mathcal{R}(q)$ and $R \coloneqq \mathcal{R}(p)$. Therefore, from (5),

$$\omega_d = \boldsymbol{\omega}_{\mathcal{D}/\mathcal{C}|\mathcal{D}} + \boldsymbol{\omega}_{\mathcal{C}/\mathcal{T}|\mathcal{D}} = \omega + Q\boldsymbol{\omega}_{\mathcal{C}/\mathcal{T}|\mathcal{C}} = \omega + Q\omega_c, \tag{6}$$

$$\hat{\omega}_d = \boldsymbol{\omega}_{\mathcal{D}/\mathcal{I}|\mathcal{D}} = \omega + Q\left(\omega_c + R\omega_t\right), \tag{7}$$

where $\omega_t \coloneqq (0, 0, n_0)$ is constant for a circular low Earth orbit with $n_0 > 0$ denoting the mean orbital motion.

B. Hybrid Systems

Hybrid systems are dynamical systems with both continuous evolution and discrete jumps [20]. A hybrid system $\mathcal{H} = (C, F, D, G)$ with state vector $\zeta \in \mathbb{R}^{n_\zeta}$ and control input $u \in \mathbb{R}^{n_u}$ is defined as a hybrid inclusion of the form

$$\mathcal{H}\begin{cases} \dot{\zeta} \in F(\zeta, u) & (\zeta, u) \in C \\ \zeta^+ \in G(\zeta, u) & (\zeta, u) \in D \end{cases} \tag{8}$$

where $C \subset \mathbb{R}^{n_\zeta} \times \mathbb{R}^{n_u}$ is the flow set, $F : \mathbb{R}^{n_\zeta} \rightrightarrows \mathbb{R}^{n_\zeta}$ is the set-valued flow map, $D \subset \mathbb{R}^{n_\zeta} \times \mathbb{R}^{n_u}$ is the jump set, and $G : \mathbb{R}^{n_\zeta} \rightrightarrows \mathbb{R}^{n_\zeta}$ is the set-valued jump map. The flow map defines the continuous dynamics of the flow set $C \subset \operatorname{dom} F$, and the jump map G defines $D \subset \operatorname{dom} G$. These objects are referred to as the data of the hybrid system $\mathcal{H}$. When the flow and jump dynamics are deterministic, the set-valued maps F and G are single valued. In that case, (8) reduces to a hybrid equation. Solutions to the hybrid system $\mathcal{H}$ are parameterized by pairs (t, j), where $t \in \mathbb{R}_{\geq 0}$ denotes ordinary time (which increases continuously during flows) and $j \in \mathbb{N}$ is a discrete counter (which increases when jumps occur). Given functions $\zeta : \operatorname{dom}\zeta \to \mathbb{R}^{n_\zeta}$ and $u : \operatorname{dom} u \to \mathbb{R}^{n_u}$, the pair (ζ, u) is a solution pair to $\mathcal{H}$ in (8) if $E \coloneqq \operatorname{dom}(\zeta, u) = \operatorname{dom}\zeta = \operatorname{dom} u$ is a hybrid time domain and the following hold: (i)$(\zeta(0,0), u(0,0)) \in C \cup D$; (ii) for each $j \in \mathbb{N}$ such that $I^j \coloneqq \{t : (t, j) \in E\}$ has nonempty interior, the map $t \mapsto \zeta(t, j)$ is locally absolutely continuous and the map $t \mapsto u(t, j)$ is Lebesgue measurable and locally essentially bounded on $\operatorname{int} I^j$; (iii) for each $j \in \mathbb{N}$ and for almost all $t \in I^j$, $(\zeta(t, j), u(t, j)) \in C$ and $d\zeta(t, j)/dt \in F(\zeta(t, j), u(t, j))$; and (iv) for each $(t, j) \in E$ such that $(t, j + 1) \in E$, $(\zeta(t, j), u(t, j)) \in D$ and $\zeta(t, j + 1) \in G(\zeta(t, j), u(t, j))$.

The set $\mathcal{S}_{\mathcal{H}}(S)$ denotes the set of all such solution pairs (ζ, u) to $\mathcal{H}$ in (8) that satisfy $\zeta(0, 0) \in S$. Given a solution pair (ζ, u), a point $(T, J) \in \operatorname{dom}(\zeta, u)$ is called its terminal (hybrid) time if $T \geq t$ and $J \geq j$ for all $(t, j) \in \operatorname{dom}(\zeta, u)$. With this terminal time (T, J), let $\{t_j\}_{j=0}^{J+1}$ satisfy $t_0 = 0$ and $t_{J+1} = T$ such that

$$E = \operatorname{dom}(\zeta, u) = \bigcup_{j=0}^{J} \Big([t_j, t_{j+1}] \times \{j\} \Big).$$

For more details on hybrid systems, please refer to [20].

C. Hybrid MPC

A set $\mathcal{T}_p \subset \mathbb{R}_{\geq 0} \times \mathbb{N}$ is called a hybrid prediction horizon if there exist a finite nonincreasing sequence $\{t_j\}_{j=0}^{J+1}$ such that $J \geq 0$ $t_0 > 0$, $t_{J+1} = T$, and

$$\mathcal{T}_p \coloneqq \bigcup_{j=0}^{J} \Big([t_{j+1},\, t_j] \times \{j\} \Big). \tag{9}$$

A natural choice that independently limits the amount of flow and the number of jumps is obtained by selecting $\delta > 0$ and $N_p \in \mathbb{N}$ and defining

$$\mathcal{T}_p \coloneqq \left\{ (T, J) \in \mathbb{R}_{\geq 0} \times \mathbb{N} \;:\; \max\{T/\delta,\; J\} = N_p \right\}. \tag{10}$$

This choice defines a rectangle of width δN_p (limiting flow to δN_p) and height N_p (restricting prediction to at most N_p jumps) with sampling parameter $\delta > 0$, and for some $N_p \in \{1, 2, \cdots\}$. With $\mathcal{T}_p$ defined in (9), consider a solution pair

(ζ, u) to $\mathcal{H}$ in (8) with hybrid terminal time $(T, J) \in \mathcal{T}_p$ and associated sequence $\{t_j\}_{j=0}^{J+1}$ satisfying $t_0 = 0$ and $t_{J+1} = T$. If $\zeta(T, J) \in X$, then the cost of the solution pair (ζ, u) is characterized by the hybrid cost functional $\mathcal{J}$ defined as

$$\mathcal{J}(\zeta, u) \coloneqq \left(\sum_{j=0}^{J} \int_{t_j}^{t_{j+1}} L_C(\zeta(t, j), u(t, j))\, dt \right) + \left(\sum_{j=0}^{J-1} L_D(\zeta(t_{j+1}, j), u(t_{j+1}, j)) \right) + V(\zeta(T, J)). \tag{11}$$

where $L_C : C \to \mathbb{R}_{\geq 0}$ is called the flow cost, $L_D : D \to \mathbb{R}_{\geq 0}$ is called the jump cost, $V : X \to \mathbb{R}_{\geq 0}$ is called the terminal cost, and X is the terminal set. The first two arguments of $\mathcal{J}$ correspond to a solution pair to $\mathcal{H}$ in (8) from ζ_0, the flow stage cost L_C defined on C, the jump cost L_D defined on D, the terminal cost V, and the terminal constraint set X. Thus, at each optimization time [23], the problem to solve is given as follows:

Problem 1 *Given the current state ζ_0, a hybrid prediction horizon $\mathcal{T}_p$, the flow stage cost L_C defined on C, the jump cost L_D defined on D, the terminal cost V defined on the terminal constraint set X,*

$$\begin{aligned} &\textit{minimize } \mathcal{J}(\zeta, u) \\ &\quad \textit{subject to} \\ &\quad \zeta(0, 0) = \zeta_0 \\ &\quad (\zeta, u) \in \mathcal{S}_{\mathcal{H}}(\zeta_0) \\ &\quad (T, J) \in \mathcal{T}_p \\ &\quad \zeta(T, J) \in X. \end{aligned} \tag{12}$$

When an optimal solution to Problem 1 exists, a minimizer $(t, j) \mapsto (\zeta^*(t, j), u^*(t, j))$ defines the value of the cost functional as $\mathcal{J}^*(\zeta_0) = \mathcal{J}(\zeta^*, u^*)$. The optimal input $(t, j) \mapsto u^*(t, j)$ with $t + j \leq T + J$ is applied over a hybrid control horizon $\mathcal{T}_c$, following the approach in [24], which mirrors the structure of the prediction horizon $\mathcal{T}_p$ in (9). Once this control input is executed, the problem is re-solved at the current state.

III. Problem Formulation

Let $x \coloneqq (\rho, \dot{\rho}, \omega, q, p, \omega_c, \rho_n, \dot{\rho}_n, x_{\text{ref}}) \in \mathbb{R}^{32}$ denote the state vector of a rigid chief-deputy spacecraft system. As defined in Section II.A, ρ and $\dot{\rho}$ are the relative docking-port displacement and velocity, respectively, ω and q are the relative angular velocity and attitude, respectively, p and ω_c are the chief attitude and angular velocity, respectively, and ρ_n and $\dot{\rho}_n$ are the composite CoM position and translational velocity in $\mathcal{T}$ frame, respectively, and $x_{\text{ref}} \coloneqq (r_{\text{des}},\ \dot{r}_{\text{des}}) \in \mathbb{R}^6$ is the state vector of an exogenous system that generates the desired orbital trajectories. Let $u \coloneqq (F_d, M_d) \in \mathbb{U} \subset \mathbb{R}^6$ denote the control input vector to the deputy with thrust vector F_d, torque moment M_d. The actuation constraint set $\mathbb{U}$ is a compact, convex set that captures the thrust and torque limits of the available actuators. Since the actuation is limited, we assume that the rendezvous and docking maneuvers take place within a constrained region indicated by the set $\mathcal{M} \subset \mathbb{R}^{32}$.

Given the above definitions of states and inputs, for each mode $h \in \Delta \coloneqq \{0, 1\}$, where $h = 0$ corresponds to the capture phase and $h = 1$ to the post-capture phase. In the capture mode $h = 0$, as the deputy approaches the docking interface, small unmitigated residual relative velocities may persist due to actuation limits and modeling uncertainties [18]. These residual velocities can lead to inadvertent low-velocity collision contacts, which are modeled as jumps. Between such contacts, the relative motion evolves continuously according to the physics of the vehicles, presented in Section IV.A. Once the relative motion has no remaining translational or rotational kinetic energy, the chief–deputy system settles into a docking configuration

$$\mathcal{A}_0 \coloneqq \{x \in \mathcal{M} : \rho = \mathbf{0},\ \dot{\rho} = \mathbf{0},\ \omega = \mathbf{0},\ q = q_I\} \tag{13}$$

where q_I is the identity quaternion, defined earlier.

Since we impose no restrictions on the chief's motion for docking to occur or on the orbital trajectory $t \mapsto x_{\text{ref}}(t)$, states p, ω_c, x_{ref} are treated as free variables, as evident from (13). Furthermore, during the capture phase ($h = 0$), ρ_n and $\dot{\rho}_n$ are computed algebraically from $(\rho, \dot{\rho}, q, p)$ and system parameters (m_c, m_d, P_c, P_d), so we do not impose separate constraints on them either. The control objective for the capture phase is to compute fuel-optimal control sequence that steer the state vector x to a prescribed small neighborhood $\mathcal{T}_{0\to1}$ around $\mathcal{A}_0$ within finite time. Once the state x enters $\mathcal{T}_{0\to1}$, the post-capture phase begins, where the objective is to stabilize the tumbling motion of the chief

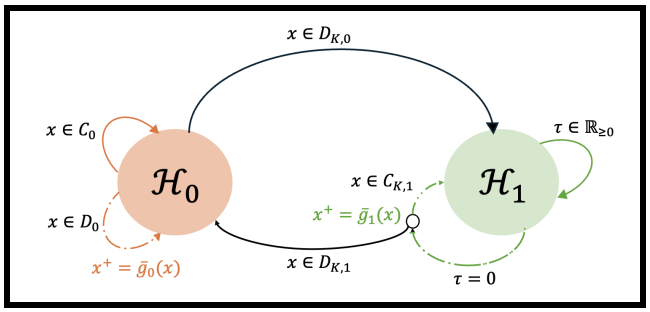

Fig. 2 Hybrid Automata for the Chief-Deputy Relative Spacecraft Dynamics.

and make the composite CoM track the desired orbital trajectory $t \mapsto x_{\text{ref}}(t)$. The control objective in mode $h = 1$ is then for $t \mapsto x(t)$ to asymptotically converge, with stability, to the set

$$\mathcal{A}_1 := \{x \in \mathcal{M} \cap \mathcal{T}_{0\to 1} : \omega_c = \mathbf{0},\ p = q_I,\ |(\rho_n, \dot{\rho}_n) - x_{\text{ref}}| = 0\}. \tag{14}$$

In the post-capture phase, inadvertent disturbances at the docking interface may induce transient decoupling. If the disturbance is sufficiently small, the resulting separation and interface loads remain below a prescribed breakaway threshold, the latch remains engaged and the system continues to operate in post capture mode. However, if the docking interface completely unlocks or fails during the post-capture phase and the relative state reaches a guard set, $\mathcal{T}_{1\to 0}$, then the composite assembly separates into two rigid bodies and the system transitions back to the capture phase.

Since such events are not directly predictable from the evolution of the state variables alone, we model their occurrence using an auxiliary timer state $\tau \in \mathbb{R}_{\geq 0}$. During flows, the timer is nonincreasing, with the magnitude of the rate of decrease no greater than one. An event is triggered once the timer reaches zero, at which point it is reset to any value in the interval $[T_1, \infty)$ where $T_1 > 0$ denotes the minimum dwell time between successive decoupling events.

The timer-induced jump (i.e., when $\tau = 0$ in mode $h = 1$) may either trigger a mode transition or merely re-initialize the post-capture evolution, depending on whether the post-jump state lies in $C_{K,1}$ or in $D_{K,1} = \mathcal{T}_{1\to 0}$. More specifically, if $\bar{g}_1(C_{K,1}) \subset C_{K,1}$, the jump keeps the system in the post-capture phase, whereas if $\bar{g}_1(C_{K,1}) \subset D_{K,1}$ it triggers a mode transition back to the capture phase. The hybrid automaton associated with this strategy is shown in Fig. 2.

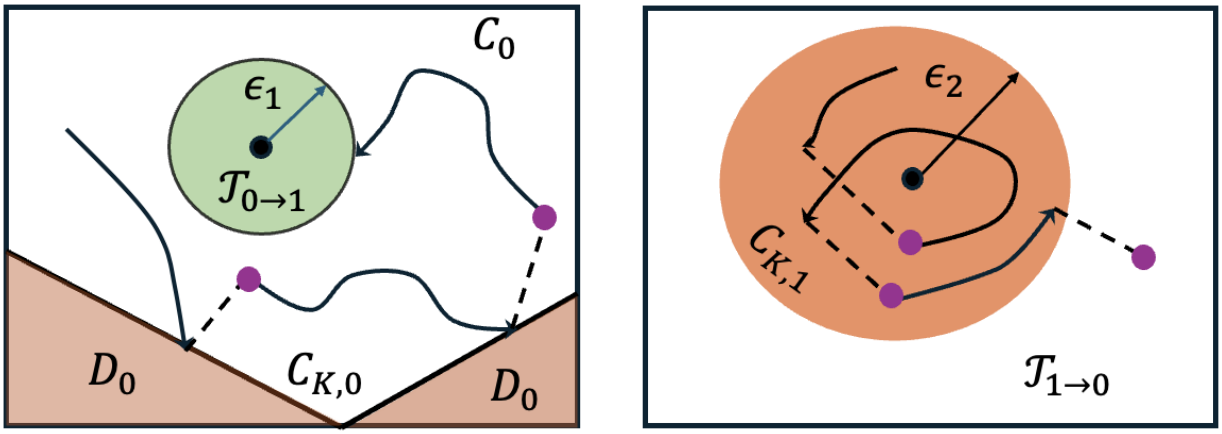

(a) $C_{K,0} = \mathcal{M} \setminus \mathcal{T}_{0\to 1} = C_0 \cup D_0$

(b) $C_{K,1} = \mathcal{M} \setminus \mathcal{T}_{1\to 0}$

Fig. 3 State-space regions for capture and post-capture operational phases.

Let $\zeta := (x, h, \tau) \in \mathcal{M} \times \mathbf{\Gamma} \times \Delta \times \mathbb{R}_{\geq 0}$ denote the augmented state. Then, for $h = 0$, the system dynamics are given

by the hybrid system

$$\mathcal{H}_0: \quad \begin{cases} \dot{\zeta} = (f_0(x,u),\, 0,\, 0) & \zeta \in \big(C_0 \cap C_{K,0}\big) \times \{0\} \times \mathbb{R}_{\geq 0} \\ \zeta^+ = \big(\bar{g}_0(x),\, h,\, \tau\big) & \zeta \in \big(D_0 \cap C_{K,0}\big) \times \{0\} \times \mathbb{R}_{\geq 0} \\ \zeta^+ = (x,\, 1-h,\, \tau) & \zeta \in D_{K,0} \times \{0\} \times \mathbb{R}_{\geq 0} \end{cases} \tag{15}$$

while, for $h = 1$,

$$\mathcal{H}_1: \quad \begin{cases} \dot{\zeta} = (f_1(x,u),\, 0,\, [-1,0]) & \zeta \in C_{K,1} \times \{1\} \times \mathbb{R}_{\geq 0} \\ \zeta^+ = \big(\bar{g}_1(x),\, h,\, [T_1,\infty)\big) & \zeta \in C_{K,1} \times \{1\} \times \{0\} \\ \zeta^+ = (x,\, 1-h,\, \tau) & \zeta \in D_{K,1} \times \{1\} \times \mathbb{R}_{\geq 0} \end{cases} \tag{16}$$

where $\mathcal{H}_0$ and $\mathcal{H}_1$ denote the capture-phase and post-capture hybrid subsystems, respectively. A mode $h \in \Delta$ is active, as long as $x \in C_{K,h}$, and once x reaches $D_{K,h}$, the mode h resets to $1-h$.

For each $h \in \Delta$, let the corresponding control law be denoted as $\kappa_{h,\text{MPC}}$ and is obtained by solving the mode-dependent MPC problems described in Section VI. A hybrid supervisory logic to robustly coordinate between these individual controllers is proposed and described as follows:

Case 1 When $h = 0$ and $x \notin \mathcal{T}_{0\to 1}$, apply the capture MPC law $u = \kappa_{0,\text{MPC}}(x)$ to drive x towards the docking configuration $\mathcal{A}_0$.

Case 2 When $h = 0$ and $x \in \mathcal{T}_{0\to 1}$, toggle the mode by setting $h^+ = 1$, i.e., post-capture mode, described in **Case** 3, becomes active.

Case 3 When $h = 1$ and $x \notin \mathcal{T}_{1\to 0}$, apply the post-capture MPC law $u = \kappa_{1,\text{MPC}}(x)$ to drive x towards $\mathcal{A}_1$ in (14).

Case 4 When $h = 1$ and $x \in \mathcal{T}_{1\to 0}$, toggle the mode by setting $h^+ = 0$, i.e., capture mode, described in **Case** 1, becomes active.

By solving a separate MPC problem of the form of Problem 1 for each $h \in \Delta$, we determine a mode-dependent MPC feedback law $\kappa_{h,\text{MPC}}$ as the minimizer of a mode-dependent objective function $J_h(\zeta, u)$, with stage costs $L_{C,h}$ and $L_{D,h}$ defined, respectively, on the flow and jump sets within $C_{K,h}$, and a terminal set X_h. The resulting hybrid feedback control input is then given by

$$u^*(\zeta) = (1-h)\,\kappa_{0,\text{MPC}}(x) + h\,\kappa_{1,\text{MPC}}(x) \qquad h \in \Delta. \tag{17}$$

IV. Relative Motion Modeling of Chief-Deputy Spacecraft Systems

In this section, we derive the rigid body models for the chief-deputy spacecraft systems for both phases. Building on the coupled translational and rotational relative motion dynamics in [13], we adapt the model to incorporate nonzero relative velocity contacts between the spacecraft, and we also extend the model to the post-capture phase.

A. Relative Translational Dynamics of the Capture Phase

The position vector of the deputy docking port relative to the docking port of the chief, as shown in Figure 1b is expressed as

$$\boldsymbol{\rho} = \boldsymbol{\rho}_0 + \boldsymbol{P}_d - \boldsymbol{P}_c. \tag{18}$$

By resolving into appropriate coordinate frames as in (5), from (18), we obtain

$$\rho_0 = R^\top(\rho + P_c) - R^\top Q^\top P_d, \tag{19}$$

$$\dot{\rho}_0 = R^\top\left[\dot{\rho} + \omega_c \times (\rho + P_c)\right] - R^\top Q^\top\left[\omega_d \times P_d\right], \tag{20}$$

where ω_c is given in (5), and ω_d in (6). Since ρ_0 is the relative displacement between the CoM of the spacecraft, as seen from frame $\mathcal{T}$, the CWH equations [25] give,

$$\ddot{\rho}_0 = G_1\rho_0 + G_2\dot{\rho}_0 + \frac{R^\top Q^\top F_d}{m_d}, \tag{21}$$

where F_d, as introduced in (5), is the thrust acting on the deputy spacecraft of mass m_d, and $G_1 = \text{diag}(3n_0^2, 0, -n_0^2)$, $G_2 = (0, 0, 2n_0)^\times$, with n_0 denoting the constant mean motion of the chief spacecraft in a circular orbit. In the case of a point-mass system, where the CoM is the only point of interest and no dedicated docking port is considered (i.e., $\rho = \rho_0$ and $P_c = \mathbf{0}_{3\times1} = P_d$), the relative translational motion between the two spacecraft is solely governed by (21). In contrast, the quantities of interest for the current scenario are $\rho, \dot{\rho}$ for the relative translational motion, and ω and $q \in \mathbb{Q}_u$ for the relative rotational motion of the chief-deputy spacecraft system. By differentiating (20) in frame $\mathcal{T}$, and by substituting (20) and (21) in place of $\dot{\rho}_0$, and $\ddot{\rho}_0$, respectively, we obtain

$$\begin{aligned}\ddot{\rho} = RG_2R^\top\dot{\rho}+RG_1R^\top\rho+\frac{Q^\top F_d}{m_d}+RG_1R^\top(P_c-Q^\top P_d) - 2\omega_c\times\dot{\rho} - \dot{\omega}_c\times(\rho+P_c) + RG_2R^\top\left[\omega_c\times(\rho+P_c)\right.\\ \left.-Q^\top(\omega+Q\omega_c)\times P_d\right] - \omega_c\times(\omega_c\times(\rho+P_c)) + Q^\top\Big[\left(\dot{\omega}+Q\left(\dot{\omega}_c - Q^\top\omega\times\omega_c\right)\right)\times P_d\\ + (\omega+Q\omega_c)\times((\omega+Q\omega_c)\times P_d)\Big] =: f_0^2(x, F_d).\end{aligned} \tag{22}$$

B. Relative Rotational Dynamics of the Capture Phase:

The dynamics of the uncontrolled chief and torque-controlled deputy spacecraft are given by

$$J_c\frac{d}{dt}|_{\mathcal{C}}\,\boldsymbol{\omega}_{C/\mathcal{I}} = -\boldsymbol{\omega}_{C/\mathcal{I}}\times\left(J_c\,\boldsymbol{\omega}_{C/\mathcal{I}}\right), \tag{23}$$

$$J_d\frac{d}{dt}|_{\mathcal{D}}\,\boldsymbol{\omega}_{\mathcal{D}/\mathcal{I}} = -\boldsymbol{\omega}_{\mathcal{D}/\mathcal{I}}\times J_d\,\boldsymbol{\omega}_{\mathcal{D}/\mathcal{I}} + M_d, \tag{24}$$

where $J_c \in \mathbb{R}^{3\times3}$ and $J_d \in \mathbb{R}^{3\times3}$ are positive definite inertia matrices for the chief and deputy, respectively, and M_d, as introduced in (5), is the control torque acting on the deputy spacecraft. Since, $\boldsymbol{\omega}_{\mathcal{D}/\mathcal{C}} = \boldsymbol{\omega}_{\mathcal{D}/\mathcal{I}} - \boldsymbol{\omega}_{C/\mathcal{I}}$, then by applying (6) and (7) to (23) and (24), we obtain

$$\dot{\omega} = J_d^{-1}\left[M_d - (\omega+Q(\omega_c+R\omega_t))\times J_d(\omega+Q(\omega_c+R\omega_t))\right] + QJ_c^{-1}\left[(\omega_c+R\omega_t)\times J_c(\omega_c+R\omega_t)\right] - Q\left(\omega_c+R\omega_t\right)\times\omega \tag{25}$$

$$=: f_0^3(\omega, q, p, \omega_c, M_d). \tag{26}$$

The relative angular velocity ω affects the orientation between frames $\mathcal{D}$ and $\mathcal{C}$, described by the quaternion $q = (q_\eta, q_\mu) \in \mathbb{Q}_u$ which evolves as

$$\left(\dot{q}_\eta, \dot{q}_\mu\right) = \frac{1}{2}\left((q_\eta^\times + q_\mu I_3)\omega, -q_\eta^\top\omega\right) =: f_0^4(q, \omega). \tag{27}$$

From (23), the evolution of the relative angular velocity ω_c between frames $\mathcal{C}$ and $\mathcal{T}$, introduced in (5), is given by

$$\dot{\omega}_c = J_c^{-1}\left(-(\omega_c+R\omega_t)^\times J_c(\omega_c+R\omega_t)\right) + \omega_c^\times R\omega_t =: f_0^5(p, \omega_c). \tag{28}$$

In turn, the angular velocity ω_c dictates the evolution of the quaternion $p = (p_\eta, p_\mu)$ described as

$$\left(\dot{p}_\eta, \dot{p}_\mu\right) = \frac{1}{2}\left(\left(p_\eta^\times + p_\mu I_3\right)\omega_c,\ -p_\eta^\top\omega_c\right) =: f_0^4(p, \omega_c). \tag{29}$$

C. Composite CoM Dynamics in the Capture Phase:

The composite CoM of the two–spacecraft system expressed in the frame $\mathcal{T}$ is given by

$$\rho_n = \frac{m_c}{m}\,\rho_c + \frac{m_d}{m}\,\rho_d, \qquad m = m_c + m_d, \tag{30}$$

where m_c and m_d denote the masses of the chief and deputy, respectively, and ρ_c and ρ_d are their CoM positions expressed in the frame $\mathcal{T}$. For $h = 0$, the chief is located at the origin of $\mathcal{T}$, so $\rho_c = 0$, and consequently $\rho_d = \rho_c+\rho_0 = \rho_0$. Hence,

$$\rho_n = \frac{m_d}{m}\,\rho_0 = \frac{m_d}{m}\left(R^\top(\rho + P_c) - R^\top Q^\top P_d\right), \tag{31}$$

with ρ_0 defined in (19). Therefore, for $h = 0$, ρ_n is an algebraic function of (ρ, p, ω_c) and is not treated as an independent state variable. The system dynamics governed by (22), (26)–(31) with states $x = (\rho, \dot{\rho}, \omega, q, p, \omega_c, \rho, \dot{\rho}_n, x_{\text{ref}}, \dot{x}_{\text{ref}}) \in \mathcal{M}$, control input $u = (u_1, u_2) \in \mathbb{U}$ with $u_1 \coloneqq F_d$, $u_2 \coloneqq M_d$, can be put into a state space form $\dot{x} = f_0(x, u)$ with

$$f_0(x,u) \coloneqq (\dot{\rho}, f_0^2(x,u_1), f_0^3(\omega, q, p, \omega_c, u_2), f_0^4(q,\omega), f_0^4(p,\omega_c), f_0^5(p,\omega_c), \dot{\rho}_n, f_0^6(x), \mathbf{0}_{6\times 1}) \tag{32}$$

where $f_0^2(x, u_1)$ is given in (22), $f_0^3(\omega, q, p, \omega_c, u_2)$ is in (26), $f_0^4(q, \omega)$ is in (27), $f_0^5(p, \omega_c)$ is in (28), and $f_0^6(x)$ is obtained from (21) and (31).

D. Rigid Body Collision Dynamics in the Capture Phase:

As the deputy spacecraft approaches the chief for docking, the presence of unmodeled disturbances, errors in the model, and inaccuracies in estimating the chief's kinematics can result in unsynchronized motion or misalignment of the docking ports, giving rise to the possibility of collision. The collision occurs if

$$v_{\text{rel}} = \hat{n}^\top \Big[\dot{\rho}_0 + R^\top Q^\top \omega \times (r - \rho_0) - (R^\top \omega_c + \omega_t) \times \rho_0 \Big] \leq 0 \tag{33}$$

where r is the position vector from the CoM of the chief to the contact point p_c, while ρ_0 and $\dot{\rho}_0$ are given in (19) and (20), respectively. The impulse vector $\hat{n}$ depends on the surface geometry at the contact point r. In the case of a frictionless collision, $\hat{n}$ acts along the surface normal direction at r. Additionally, v_{rel} in (33) can be formulated as a function of the state vector x^0, exogenous inputs w^0, and the contact point r as $v_{\text{rel}} = \beta(x, \sigma)$, where β can be viewed as an impact condition function with $\sigma \coloneqq (r, \hat{n})$ being a vector external parameters r and $\hat{n}$.

With an impulse magnitude γ along the direction $\hat{n}$, the instantaneous change in the relative angular velocity ω between frames $\mathcal{D}$ and C, and ω_c between frames C and $\mathcal{T}$, can be evaluated as

$$\omega^+ = \omega + \gamma \left[J_d^{-1} Q R \big((r - \rho_0) \times \hat{n} \big) + Q J_c^{-1} R \big(r \times \hat{n} \big) \right] =: \bar{g}_0^3(x), \qquad \omega_c^+ = \omega_c - \gamma J_c^{-1} R (r \times \hat{n}) =: \bar{g}_0^4(p, \omega_c). \tag{34}$$

Such an instantaneous change in the angular velocities ω and ω_c in (34) induces an instantaneous change in the evolution of the quaternions q in (27) and p in (29) as

$$\dot{q}^+ = f_0^4(\omega^+, q), \;\; \dot{p}^+ = f_0^4(\omega_c^+, p), \tag{35}$$

where $f_0^4(\omega, q)$ is given in (27), and $f_0^4(\omega_c, p)$ in (29).The instantaneous change in the relative translational velocity $\dot{\rho}_0$ in (19) can be obtained as

$$\dot{\rho}_0^+ = \dot{\rho}_0 + \gamma \hat{n} \left(\frac{1}{m_d} + \frac{1}{m_c} \right). \tag{36}$$

Since $\dot{\rho}_0^+ = R^\top \left[\dot{\rho}^+ + \omega_c^+ \times (\rho + P_c) \right] - R^\top Q^\top \left[\omega_d^+ \times P_d \right]$ from (20), where $\omega_d^+ = \omega^+ + Q\omega_c^+$, then

$$\dot{\rho}^+ = \dot{\rho} + \omega_c \times (\rho + P_c) - Q^\top (\omega_d \times P_d) + \gamma R \hat{n} \left(\frac{1}{m_d} + \frac{1}{m_c} \right) + Q^\top \big(Q\omega_c^+ \times P_d \big) - \omega_c^+ \times (\rho + P_c) + Q^\top (\omega^+ \times P_d) =: \bar{g}_0^2(x), \tag{37}$$

with ω^+ and ω_c^+ given in (34). Furthermore, by using (36), we obtain

$$\dot{\rho}_n^+ = \dot{\rho}_n + \frac{\gamma}{m_c} \hat{n} =: \bar{g}_0^5(x). \tag{38}$$

The overall system dynamics after an instantaneous change, can be put into the state space form $x^+ = g_0(x)$ with

$$\bar{g}_0(x) \coloneqq (\rho, \bar{g}_0^2(x), \bar{g}_0^3(x), q, p, \bar{g}_0^4(p, \omega_c), \rho_n, \bar{g}_0^5(x), x_{\text{ref}}) \tag{39}$$

where $\bar{g}_0^2(x)$ is given in (37), $\bar{g}_0^3(x)$ and $\bar{g}_0^4(p, \omega_c)$ are in (34), and $\bar{g}_0^5(x)$ is in (38).

E. Relative Translational and Rotational Dynamics in Post-Capture Phase:

When x reaches the set $\mathcal{T}_{0\to1}$, the post–capture phase ($h = 1$) begins. In this phase, the docking interface employs a spring–damper latching mechanism to enable soft docking and absorb the residual relative translational and rotational motion. The translational compliance is characterized by the spring and damping coefficients $K_T > 0$ and $D_T > 0$, while $K_R > 0$ and $D_R > 0$ denote the corresponding torsional spring and damping coefficients for the rotational motion, as shown in Figure 4.

Under the passive control action provided by the docking interface in $h = 1$, which (i) absorbs the residual translational and rotational energy and (ii) renders the docked configuration $\mathcal{A}_0$ in (13) invariant, the relative translational dynamics are described as

$$\begin{aligned}\ddot{\rho} = &-K_T\rho - D_T\dot{\rho} + RG_2R^\top\dot{\rho}+RG_1R^\top\rho+\frac{Q^\top u_1^*}{m_d}+RG_1R^\top(P_c-Q^\top P_d) - 2\omega_c\times\dot{\rho} - \dot{\omega}_c\times(\rho+P_c)\\ &+RG_2R^\top\left[\omega_c\times(\rho+P_c) - Q^\top(\omega+Q\omega_c)\times P_d\right] - \omega_c\times(\omega_c\times(\rho+P_c)) + Q^\top\Big[\left(\dot{\omega}+Q\left(\dot{\omega}_c - Q^\top\omega\times\omega_c\right)\right)\times P_d\Big]\\ &+ Q^\top\Big[(\omega+Q\omega_c)\times((\omega+Q\omega_c)\times P_d)\Big] =: f_1^2(x),\end{aligned} \tag{40}$$

where F_d in (22) has been replaced by $Q(-K_T\rho - D_T\dot{\rho}) + \bar{u}_1$, steady state control (the value of $\bar{u}_1$, defined just before (32), at the docking configuration $\rho = \mathbf{0},\ \dot{\rho} = \mathbf{0},\ \omega = \mathbf{0},\ q = q_I$)

$$\bar{u}_1 = m_d\Big[-RG_1R^\top(P_c - P_d)+\dot{\omega}_c^\times(P_c - P_d) + \omega_c^\times\left(\omega_c^\times(P_c - P_d)\right) - RG_2R^\top\left(\omega_c^\times(P_c - P_d)\right)\Big] =: \kappa_1^0(p,\omega_c). \tag{41}$$

Inspired by local PD–type attitude control laws for rigid spacecraft [26],[27, Pg.21], the relative rotational dynamics can likewise be obtained by introducing a torsional spring–damper about the docking interface. Replacing M_d in (26) with $-\frac{2}{|q|}\arctan\left(|q|, q_4\right) K_R\, q - D_R\omega + \bar{u}_2$ yields

$$\begin{aligned}\dot{\omega} = J_d^{-1}\Big(&-\frac{2}{|q|}\arctan\left(|q|, q_4\right)\ K_R\, q - D_R\omega + u_2^* - (\omega + Q(\omega_c + R\omega_t))\times J_d(\omega + Q(\omega_c + R\omega_t))\Big)\\ &- Q(\omega_c + R\omega_t)\times\omega + QJ_c^{-1}\Big((\omega_c + R\omega_t)\times J_c(\omega_c + R\omega_t)\Big) =: f_1^3(\omega, q, p, \omega_c),\end{aligned} \tag{42}$$

where the steady control torque (the value of u_2, defined just before (32), at the docking configuration $\rho = \mathbf{0},\ \dot{\rho} = \mathbf{0},\ \omega = \mathbf{0},\ q = q_I$)

$$\bar{u}_2 = \left[(\omega_c + R\omega_t)^\times J_d\,(\omega_c + R\omega_t)\right] - J_d\, J_c^{-1}\left[(\omega_c + R\omega_t)^\times J_c(\omega_c + R\omega_t)\right] =: \kappa_2^0(p,\omega_c). \tag{43}$$

to maintain the nominal docked attitude.

F. Translational and Rotational Dynamics in the Post-Capture Phase

With combined mass $m = m_c + m_d$ and moments of inertia $J := J_c + J_d$ for the post-capture phase, we now derive the equations of motion of the composite chief-deputy spacecraft system, as shown in Figure 4. Let the position vector to the CoM of the deputy be denoted as $\boldsymbol{r}_1$ and to the CoM of the chief be $\boldsymbol{r}_2$ with $\boldsymbol{r}_1 = \boldsymbol{r}_1 + \boldsymbol{\rho}_0$ where ρ_0 is the vector connecting the CoMs of both the spacecraft. Let $\boldsymbol{r}_n$ denote the center of mass (CoM) of the combined chief–deputy system, defined as

$$\boldsymbol{r}_n = \frac{m_c\boldsymbol{r}_2 + m_d\boldsymbol{r}_1}{m}. \tag{44}$$

Since the actuation $\boldsymbol{F}_d$ is applied at the deputy CoM, the inertial translational dynamics of the chief and deputy are described as

$$\ddot{\boldsymbol{r}}_2 = -\frac{\mu}{R_2^3}\boldsymbol{r}_2, \qquad \ddot{\boldsymbol{r}}_1 = -\frac{\mu}{R_1^3}\boldsymbol{r}_1 + \frac{\boldsymbol{F}_d}{m}, \tag{45}$$

and thus, the composite CoM dynamics from (44)–(45) are given by

$$\ddot{\boldsymbol{r}}_n = \frac{m_c}{m}\ddot{\boldsymbol{r}}_2 + \frac{m_d}{m}\ddot{\boldsymbol{r}}_1 = -\frac{\mu}{m}\left(\frac{m_c}{R_2^3}\boldsymbol{r}_2 + \frac{m_d}{R_1^3}\boldsymbol{r}_1\right) + \frac{\boldsymbol{F}_d}{m}, \tag{46}$$

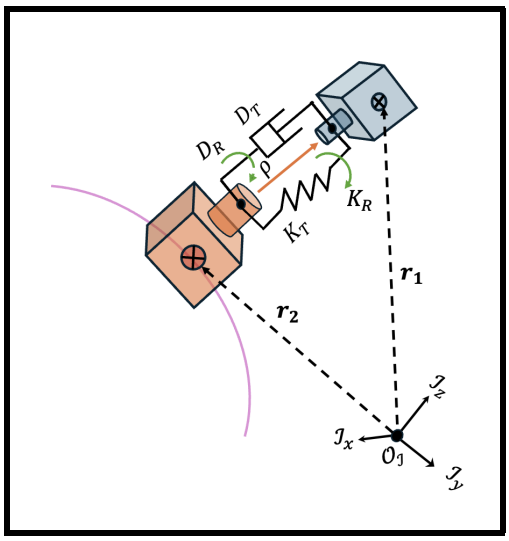

(a) spring-damper docking interface

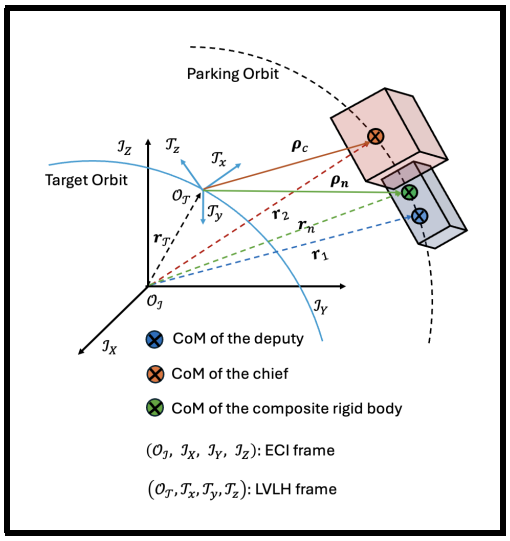

(b) Combined chief–deputy assembly in the post–capture phase

Fig. 4 Representative schematics for the capture and post–capture operational phases.

where μ is Earth's gravitational constant, $R_i := |\boldsymbol{r}_i|$ for each $i \in \{1, 2\}$ and $R_n := |\boldsymbol{r}_n|$. Since $|\rho_0| \ll R_n$, from (46), we obtain

$$\ddot{\boldsymbol{r}}_n \approx -\frac{\mu}{m\|\boldsymbol{r}_n\|^3}\left(m_c\left(\boldsymbol{r}_n - \frac{m_d}{m}\boldsymbol{\rho}\right) + m_d\left(\boldsymbol{r}_n + \frac{m_c}{m}\boldsymbol{\rho}\right)\right) + \frac{\boldsymbol{F}_d}{m} = -\mu\,\frac{\boldsymbol{r}_n}{\|\boldsymbol{r}_n\|^3} + \frac{\boldsymbol{F}_d}{m}. \tag{47}$$

As introduced in (5), let us recall that $\boldsymbol{\rho}_n$ is the position vector of the combined spacecraft CoM in the LVLH frame $\mathcal{T}$, which has the origin at the initial target orbit. Let $\rho_n := \boldsymbol{\rho}_n\big|_\mathcal{T}$, then following the same steps as in Section IV.A to arrive at (21), results in

$$\ddot{\rho}_n = G_1\rho_n + G_2\dot{\rho}_n + \frac{R^\top F_d}{m} =: f_1^6(\rho_n, \dot{\rho}_n, p, F_d), \tag{48}$$

where the matrices G_1 and G_2 are defined below (21). Next, we derive the rotational dynamics of the composite rigid spacecraft system.

Let $\boldsymbol{\rho}_c$ denote the position vector of the chief CoM from the origin of frame $\mathcal{T}$, as illustrated in Figure 4. Similarly, let $\boldsymbol{\rho}_c$ denote the deputy CoM from the origin of $\mathcal{T}$. Then, the rotational dynamics of the composite system under the torque $\boldsymbol{M}_d \in \mathbb{R}^3$, and the force moment due to the shift in the CoM be given as

$$J\frac{d}{dt}\Big|_C \boldsymbol{\omega}_{C/\mathcal{I}} = -\boldsymbol{\omega}_{C/\mathcal{I}} \times \left(J\,\boldsymbol{\omega}_{C/\mathcal{I}}\right) + \boldsymbol{M}_d + (\boldsymbol{r}_1 - \boldsymbol{r}_n)^\times \boldsymbol{F}_d. \tag{49}$$

Since $\boldsymbol{\omega}_{C/\mathcal{I}|C} = \boldsymbol{\omega}_{C/\mathcal{T}|C} + \boldsymbol{\omega}_{\mathcal{T}/\mathcal{I}|C} = \omega_c + R\omega_{\mathcal{T}/\mathcal{I}|\mathcal{T}} = \omega_c + R\omega_t$ where ω_t is constant on a circular orbit, and

$$\begin{aligned}\frac{d}{dt}\Big|_\mathcal{I}\boldsymbol{\omega}_{C/\mathcal{I}} = \frac{d}{dt}\Big|_C\boldsymbol{\omega}_{C/\mathcal{I}} = \frac{d}{dt}\Big|_C\left[\boldsymbol{\omega}_{C/\mathcal{T}} + \boldsymbol{\omega}_{\mathcal{T}/\mathcal{I}}\right] = \dot{\omega}_c + \left[\frac{d}{dt}\Big|_\mathcal{T}(\boldsymbol{\omega}_{\mathcal{T}/\mathcal{I}}) + \boldsymbol{\omega}_{\mathcal{T}/C} \times \boldsymbol{\omega}_{\mathcal{T}/\mathcal{I}}\right]\Big|_C \\ = \dot{\omega}_c + \boldsymbol{\omega}_{\mathcal{T}/C|C} \times \boldsymbol{\omega}_{\mathcal{T}/\mathcal{I}|C} = \dot{\omega}_c - \omega_c^\times\,(R\omega_t)\,,\end{aligned} \tag{50}$$

then, by using (49)–(50), the rotational dynamics is obtained as

$$\dot{\omega}_c = \omega_c^\times\,(R\omega_t) + J^{-1}\left[-(\omega_c + R\omega_t)^\times J(\omega_c + R\omega_t) + M_d + \frac{m_c}{m}(P_c - P_d)^\times F_d\right] =: f_1^5(p, \omega_c, F_d, M_d). \tag{51}$$

The system dynamics governed by (40), (42), (48), and (51) with states $x \in \mathcal{M}$, control input $u = (u_1, u_2) \in \mathbb{U}$ with $u_1 = F_d$, $u_2 = M_d$, can be put into the state space form $\dot{x} = f_1(x, u)$ with

$$f_1(x, u) := \left(\dot{\rho}, f_1^2(x), f_1^3(\omega, q, p, \omega_c), f_0^4(q, \omega), f_0^4(p, \omega_c), f_1^5(p, \omega_c, u), \dot{\rho}_n, f_1^6(\rho_n, \dot{\rho}_n, p, u_1), f_\mathcal{T}(x_{\text{ref}})\right) \tag{52}$$

where $f_1^2(x)$ is given in (40), $f_1^3(\omega, q, p, \omega_c)$ is given in (42), $f_0^4(q, \omega)$ is in (27), $f_0^4(p, \omega_c)$ in (29), $f_1^5(p, \omega_c, u)$ is in (51), and $f_1^6(\rho_n, \dot{\rho}_n, p, u_1)$ is in (48).

G. Decoupling Dynamics in the Post-Capture Phase

In the post-capture phase, internal disturbances or the release of stored energy may give rise to equal and opposite forces on the two spacecraft, tending to break the docked configuration. Since the impulse acts along the docking interface,

$$\omega_c^+ = \omega_c, \tag{53}$$

that is, the angular velocity of the composite body expressed in $\mathcal{T}$ is unaffected by the impulse. Consequently, the relative angular velocity between the frames $\mathcal{C}$ and $\mathcal{D}$ immediately after the jump is given as

$$\omega^+ = \omega \tag{54}$$

where ω is defined in (5). Additionally, an instantaneous change in the angular velocities ω_c and ω in (53) and (54), respectively, induces an instantaneous change in the evolution of the quaternions q in (27) and p in (29) as

$$\dot{q}^+ = f_0^4(\omega^+, q) = f_0^4(\omega, q) = \dot{q}, \qquad\qquad \dot{p}^+ = f_0^4(\omega_c^+, p) = f_0^4(\omega_c, p) = \dot{p}, \tag{55}$$

where q is an identity quaternion q_I in the docked configuration.

The relative translational velocity between the chief and deputy at the jump is given by

$$\dot{\rho}_0^+ = \dot{\rho}_0 - T_\pi \left(\frac{1}{m_c} + \frac{1}{m_d} \right). \tag{56}$$

while the translational motion of the individual CoMs as

$$\dot{\rho}_c^+ = \dot{\rho}_c + \frac{1}{m_c} T_\pi, \qquad \dot{\rho}_d^+ = \dot{\rho}_d - \frac{1}{m_d} T_\pi. \tag{57}$$

where T_π is the impulse force, expressed in frame $\mathcal{T}$, and Since $\rho_n = \frac{m_c\rho_c + m_d\rho_d}{m} = \rho_c + \frac{m_d}{m}\rho_0$, from (56), we obtain

$$\dot{\rho}_n^+ = \dot{\rho}_c^+ + \frac{m_d}{m}\dot{\rho}_0^+ = \dot{\rho}_c + \frac{1}{m_c} T_\pi + \frac{m_d}{m}\dot{\rho}_0 - \frac{m_d}{m}\left(\frac{1}{m_c} + \frac{1}{m_d} \right) T_\pi = \left(\dot{\rho}_c + \frac{m_d}{m}\dot{\rho}_0 \right) = \dot{\rho}_n. \tag{58}$$

Furthermore, from (19)–(20), the post-impulse relative translational velocity between the docking ports satisfies

$$\dot{\rho}_0^+ = (R^+)^\mathsf{T} \left[\dot{\rho}^+ + \omega_c^+ \times (\rho^+ + P_c) \right] - (R^+)^\mathsf{T} (Q^+)^\mathsf{T} \left[\omega_d^+ \times P_d \right]. \tag{59}$$

Since the angular velocities, relative displacements, and orientations between the bodies do not change instantaneously, i.e., $\omega_c^+ = \omega_c$, $\omega_d^+ = \omega_d$ from (53), $\rho^+ = \rho$, $R^+ = R$, and $Q^+ = Q$, (59) yields

$$\dot{\rho}_0^+ - \dot{\rho}_0 = R^\mathsf{T}(\dot{\rho}^+ - \dot{\rho}), \qquad \dot{\rho}^+ = \dot{\rho} - R \left(\frac{1}{m_c} + \frac{1}{m_d} \right) T_\pi =: \bar{g}_1^2(x). \tag{60}$$

The overall system dynamics (53)–(54), (58), and (60) after an instantaneous change can be written in the state-space form $x^+ = \bar{g}_1(x)$ where

$$\bar{g}_1(x) \coloneqq \left(\rho, \bar{g}_1^2(x), \omega, q, p, \omega_c, \rho_n, \dot{\rho}_n, x_{\text{ref}} \right), \tag{61}$$

with $\bar{g}_1^2(x)$ defined in (60).

V. Constraints Formulation for MPC

Recall that we solve a different MPC problem in each mode of operation corresponding to $h \in \Delta$. Then, recalling the full state x from Section III, we partition the state x as $x = (x^0, x^1, x_{\text{ref}})$, where

$$x^0 \coloneqq (\rho, \dot{\rho}, \omega, q) = \Psi_0(x), \qquad\qquad x^1 \coloneqq (p, \omega_c, \rho_n, \dot{\rho}_n) = \Psi_1(x), \tag{62}$$

and $\Psi_0, \Psi_1 : \mathbb{R}^{32} \to \mathbb{R}^{13}$ denote the respective canonical projection maps. In each mode $h \in \Delta$, x^h, together with the control u, appear as decision variables in the MPC optimization, while the remaining states evolve according to the

nonlinear dynamics and act as time-varying parameters. In particular, when $h = 0$ (resp. $h = 1$), the component x^1 (resp. x^0) evolves according to the nonlinear dynamics in (32) (resp., the passive PD feedback law from Section IV.E).

For ease of MPC computation, we linearize the nonlinear dynamics associated to x^0 (resp., x^1) in phase $h = 0$ (resp., $h = 1$) about the docking configuration $\Psi_0(\mathcal{A}_0)$ (resp., $\Psi_1(\mathcal{A}_1)$), where we recall $\mathcal{A}_0$ and $\mathcal{A}_1$ from (13) and (14), respectively. For each $h \in \Delta$, the linearization uses the state $\delta x^h := x - x^h$ and the input $\delta u^h := u - u^h$, where u^h is the steady-state input. In particular, $u^0 := (\kappa_1^0(p, \omega_c), \kappa_2^0(p, \omega_c))$, where $\kappa_1^0(p, \omega_c)$ is defined in (41) and $\kappa_2^0(p, \omega_c)$ in (43), and $u^1 := (\kappa_1^1(x_{\text{ref}}), \kappa_2^1(x_{\text{ref}}))$, where $\kappa_1^1(x_{\text{ref}})$ and $\kappa_2^1(x_{\text{ref}})$ are defined in (65). Accordingly, the linearized system dynamics in the capture phase are parameterized by (p, ω_c), whereas in the postcapture phase they are parameterized by x_{ref}.

A. Actuation Constraints in the Capture Phase:

Due to the finite thrusting capability of the deputy spacecraft, the control constraint set $\mathbb{U}$ is formulated as $\mathbb{U} := \{u \in \mathbb{R}^6 : -u_{\max} \leq u \leq u_{\max}\}$, where $u_{\max} \in \mathbb{R}^6$ defines the maximum thrust and torque limit in three axial directions of the deputy's body frame $\mathcal{D}$. Equivalently, δu^0 is constrained using the following set:

$$\delta\mathbb{U}^0(p, \omega_c) := \{\delta u^0 \in \mathbb{R}^6 : \delta u^0 + \kappa^0(p, \omega_c) \in \mathbb{U}\}. \tag{63}$$

where $\kappa^0(p, \omega_c) := (\kappa_1^0(p, \omega_c), \kappa_2^0(p, \omega_c))$ and the functions κ_1^0 and κ_2^0 are defined in (41) and (43), respectively. For the postcapture phase, equivalently, the actuation constraint on δu^1 can be written as

$$\delta\mathbb{U}^1(x_{\text{ref}}) := \{\delta u^1 \in \mathbb{R}^6 : \delta u^1 + \kappa^1(x_{\text{ref}}) \in \mathbb{U}\}, \tag{64}$$

where $\kappa^1(x_{\text{ref}}) := \big(\kappa_1^1(x_{\text{ref}}), \kappa_2^1(x_{\text{ref}})\big)$, and $\kappa_1^1(x_{\text{ref}})$ and $\kappa_2^1(x_{\text{ref}})$ are defined as follows:

$$\kappa_1^1(x_{\text{ref}}) = m\Big(f_{T,2}(x_{\text{ref}}) - G_1 \begin{bmatrix} I_3 & 0 \end{bmatrix} x_{\text{ref}} - G_2 f_{T,1}(x_{\text{ref}})\Big), \qquad \kappa_2^1(x_{\text{ref}}) = \omega_t^\times J\omega_t - \frac{m_c}{m}(P_c - P_d)^\times \hat{u}_1. \tag{65}$$

with $\dot{x}_{\text{ref}} = f_T(x_{\text{ref}})$, where $f_T := (f_{T,1}, f_{T,2})$ defines the evolution of the desired orbital reference.

B. Face Pointing Constraints:

The deputy spacecraft must approach the target while oriented towards its docking port during the capture phase. This requirement is enforced as a soft constraint by augmenting the MPC cost function with the term:

$$\mathcal{V}(\delta x^0, p, \omega_c, v) := \lambda_f(|\delta\rho| - v^\top R^\top \delta\rho)^2, \tag{66}$$

where $\lambda_f > 0$ is a weighting factor, and $v := P_c/|P_c|$ is the normal vector on the docking face of the chief spacecraft in frame $\mathcal{T}$, as shown in Figure 4. Here, P_c, defined in (5), denotes the position vector from the CoM of the chief to its docking port. As $|\delta\rho|$ decreases for docking, this penalty term (66) encourages the alignment of $R^\top\delta\rho$ with the normal vector v.

VI. MPC Design

In this section, we design an MPC controller for each phase $h \in \Delta$. Each hybrid MPC controller uses a linearized prediction model together with the phase-specific constraints.

A. Capture-Phase MPC

Our proposed MPC framework defines a controller for the capture phase using the capture phase linearized dynamics with state variables δx^0 and input δu^0, actuation constraints (63), and LoS tracking penalty (66). Let us define the prediction horizon as $\mathcal{T}_p^0 := (T^0, J^0)$, where $T^0 > 0$ is the terminal flow time and $J^0 > 0$ is the number of jumps. Then, the control law $\kappa_{0,\text{MPC}}$ is generated by solving the following optimization problem.

Problem 2 *Given the current state δx_0^0, a prediction horizon $\mathcal{T}_p^0 \in \mathbb{R}_{\geq 0} \times \mathbb{N}$, stage flow cost L_C^0, jump cost L_D^0, terminal cost V^0, and actuation constraint set $\delta\mathbb{U}^0$, the optimal control $\kappa_{0,MPC}$ is obtained by solving the following optimization problem:*

$$\min_{\delta u^0} \mathcal{J}^0(\delta x^0, \delta u^0, p, \omega_c) \tag{67}$$

subject to

(*I*) *Initial condition* $\quad \delta x^0(0) = \delta x_0^0$ (68)

(*II*) *Linearized capture flow-dynamics* $\quad \dot{\delta x^0} = \tilde{A}(p, \omega_c)\, \delta x^0 + \tilde{B}\, \delta u^0$ (69)

(*III*) *Input constraints* $\quad \delta u^0 \in \delta \mathbb{U}^0(p, \omega_c)$ (70)

$$\begin{aligned} \mathcal{J}^0(\delta x^0, \delta u^0, p, \omega_c, c) \coloneqq & \sum_{j=0}^{J^0} \int_{t_j}^{t_{j+1}} L_C^0(\delta x^0(t, j), \delta u^0(t, j), p(t, j), \omega_c(t, j), c)\, dt \\ & + \sum_{j=0}^{J^0} L_D^0(\delta x^0(t_{j+1}, j), \delta u^0(t_{j+1}, j)) + V^0(\delta x^0(T^0, J^0), c). \end{aligned} \tag{71}$$

The decision variables are δx^0, and δu^0, while p and ω_c are external time-varying parameters to the optimization problem, that evolve as per the flow map given in (28)–(29), and $c > 0$ denotes the number of collisions experienced during capture. Moreover, $\tilde{A}$ and $\tilde{B}$, parameterized by (p, ω_c), are the state and input matrices of the capture phase linearized state-space model (69). While the prediction model employed in Problem 2 is the continuous-time linear system (69), the true closed-loop dynamics of the chief-deputy system are governed by the nonlinear hybrid dynamics, with flow and jump maps given in (32) and (39), respectively. The nonlinear dynamics are used to propagate the system state forward in time and to compute the new initial condition for the MPC optimization upon application of the computed control input.

Design of $\bar{Q}^0$: Since the contacts occur at time instants that are not a priori known, the jump cost and the number of jumps cannot be explicitly accounted for in Problem 2. Therefore, both L_D^0 and J^0 are set to zero in (71). Our choices of L_C^0 and V^0 are given as

$$V^0(\delta x^0, c) \coloneqq (\delta x^0)^\top Q_{\mathrm{f}}^0(c)\, \delta x^0,\ L_C^0(\delta x^0, \delta u^0, p, \omega_c, c) \coloneqq (\delta x^0)^\top \bar{Q}^0(c)\, \delta x^0 + (\delta u^0)^\top \bar{R}^0\, \delta u^0 + \mathcal{V}(\delta x^0, p, \omega_c, v), \tag{72}$$

where $Q_{\mathrm{f}}^0, \bar{R}^0 \succ \mathbf{0}$, $\bar{Q}^0(c) \succ \mathbf{0}$ for each $c \geq 0$, and $\mathcal{V}$ is given in (66). The penalty matrix $\bar{Q}^0$ is adjusted as a function of c, such that increasing collision count results in larger penalties on $\delta\dot{\rho}$, $\delta\omega$, and δq_η. Since the rotational dynamics evolve independently while the translational motion is driven by the rotational state, penalizing the rotational components more heavily accelerates their convergence and effectively decouples the optimization problem into rotational and translational subproblems. Thus, the stage cost assigns higher weights to the relative angular velocity $\delta\omega$ and orientation error δq_η than to the relative displacement $\delta\rho$ and translational velocity $\delta\dot{\rho}$.

Design of $Q_{\mathbf{f}}^0$: The weighting matrix $Q_{\mathrm{f}}^0 \succ \mathbf{0}$ in (72) is selected to satisfy the standard Lyapunov-based MPC terminal conditions [23]. In particular, Q_{f}^0 is chosen such that V^0 in (72) acts as a Lyapunov function for the closed-loop system under the admissible terminal feedback law $\delta u^0 = K_0\, \delta x^0 \in \delta \mathbb{U}^0(p, \omega_c)$. As a result, the closed-loop linearized capture-flow dynamics (69) satisfy a strict dissipation (contractivity) inequality and induce a locally invariant terminal region $\mathcal{X}_f^0(c)$ for the actual nonlinear system (32). For each $c > 0$, the terminal set $\mathcal{X}_f^0(c)$ is defined as a sufficiently small sublevel set of V^0, i.e., $\mathcal{X}_f^0(c) = \{\delta x^0 : V^0(\delta x^0, c) \leq \varepsilon_c\}$ where $\varepsilon_c > 0$ is chosen small enough so that higher-order nonlinear terms and linearization-mismatch effects are dominated by the contraction induced by the terminal feedback δu^0.

B. Post-Capture Phase MPC

Following the successful capture, the closed-loop system enters the post-capture phase ($h = 1$), during which the chief–deputy system becomes coupled and the state vector x of the coupled system evolves according to the dynamics (52). In this phase, the control objectives are to synthesize the control law $\kappa_{1,\mathrm{MPC}}$ that asymptotically stabilizes the set $\mathcal{A}_1$ in (14). Let the prediction horizon be denoted by $\mathcal{T}_p^1 \coloneqq (T^1, J^1)$, where $T^1 > 0$ is the terminal flow time and $J^1 > 0$ is the number of jumps.

Problem 3 *Given the current state δx_0^1, a prediction horizon $\mathcal{T}_p^1 \in \mathbb{R}_{\geq 0} \times \mathbb{N}$, stage flow cost L_C^1, jump cost L_D^1, terminal cost V^1, and actuation constraint set $\delta\mathbb{U}^1$, the optimal control κ_{MPC}^1 is obtained by solving*

$$\min_{\delta u^1} \mathcal{J}^1(\delta x^1, \delta u^1, x_{\text{ref}}) \tag{73}$$

subject to

$$(I)\ \textit{Initial condition} \quad \delta x^1(0) = \delta x_0^1 \tag{74}$$

$$(II)\ \textit{Linearized post-capture flow-dynamics} \quad \dot{\delta x^1} = \hat{A}(x_{\text{ref}})\, \delta x^1 + \hat{B}\, \delta u^1 \tag{75}$$

$$(III)\ \textit{Input constraints} \quad \delta u^1 \in \delta\mathbb{U}^1(x_{\text{ref}}) \tag{76}$$

where the cost functional is defined as

$$\mathcal{J}^1(\delta x^1, \delta u^1, x_{\text{ref}}) \coloneqq \sum_{j=0}^{J^1} \int_{t_j}^{t_{j+1}} L_C^1\big(\delta x^1(t,j), \delta u^1(t,j), x_{\text{ref}}(t,j)\big)\, dt + \sum_{j=0}^{J^1} L_D^1\big(\delta x^1(t_{j+1}, j), \delta u^1(t_{j+1}, j)\big) + V^1\big(\delta x^1(T^1, J^1)\big),$$

$$V^1(\delta x^1) \coloneqq (\delta x^1)^\top Q_{\text{f}}^1 \delta x^1,\ L_C^1(\delta x^1, \delta u^1, x_{\text{ref}}) \coloneqq \begin{bmatrix} \delta p_\eta & \delta\omega_c \end{bmatrix}^\top \bar{Q}_1^1 \begin{bmatrix} \delta p_\eta \\ \delta\omega_c \end{bmatrix} + \begin{bmatrix} \delta\rho_n & \dot{\delta\rho}_n \end{bmatrix}^\top \bar{Q}_2^1 \begin{bmatrix} \delta\rho_n \\ \dot{\delta\rho}_n \end{bmatrix} + (\delta u^1)^\top \bar{R}^1 (\delta u^1), \tag{77}$$

with $\bar{Q}_i^1 \succ \mathbf{0}$ for $i \in \{1, 2\}$, $\bar{R}^1 \succ \mathbf{0}$, $Q_f^1 \succ \mathbf{0}$. Moreover, the matrices $\hat{A}$ and $\hat{B}$, parameterized by x_{ref} in (75), are the state and input matrices of the post-capture linearized state-space model. The decision variables are δx^1 and δu^1, while x^0 and x_{ref} are treated as parameters of the optimization problem. Since the jumps due to sudden decoupling events occur at time instants that are not known a priori, both L_D^1 and J^1 are set to zero in (77).

Design of $\bar{Q}_1^1, \bar{Q}_2^1$: The weighting matrices are chosen to prioritize penalizing the rotational components more heavily, which accelerates their convergence and effectively decouples the optimization problem into rotational and translational subproblems, analogous to the capture-phase MPC in Section VI.A.

Design of Q_{f}^1: The terminal weight $Q_{\text{f}}^1 \succ \mathbf{0}$ in (77) for the post-capture MPC is selected analogously to the capture phase, following standard Lyapunov-based MPC terminal conditions to ensure local attractivity and recursive feasibility. In particular, Q_{f}^1 is chosen so that V^1 acts as a Lyapunov function for the local error dynamics under an admissible terminal control law $\delta u^1 = K_1\, \delta x^1$. The terminal set $\mathcal{X}_f^1$ is selected to be sufficiently small so that the Lyapunov decrease induced by δu^1 dominates the model-mismatch.

If external disturbances or modeling errors cause loss of the rigid lock, and the augmented state reaches the transition set $\mathcal{T}_{1\to 0}$, the logic variable h updates from one to zero, and the system re-enters the capture phase, at which point Problem 3 is re-solved.

VII. Numerical Results

In this section, we present a numerical example to illustrate the effectiveness of the proposed control design for each phase. Both the chief and deputy spacecraft are modeled as constant density cuboids with dimensions 0.6 m × 0.7 m × 0.8 m for the deputy and 1.04 m × 1.15 m × 1.57 m for the chief. The inertia matrices J_c and J_d are diagonal, since the cuboids are assumed to be symmetric about the principal axes of their respective body frames. In this simulation, the initial conditions are as follows:

$$\begin{aligned} &\rho_0(0,0) = \begin{bmatrix} 2 & 0 & 0 \end{bmatrix}^\top,\ \dot{\rho}_0 = \begin{bmatrix} -0.081 & 0.011 & 0.0133 \end{bmatrix}^\top, \\ &\omega(0,0) = \begin{bmatrix} 0.09 & 0.06 & 0.009 \end{bmatrix}^\top,\ q(0,0) = 0.57 \begin{bmatrix} \mathbf{1}_3^\top & 0 \end{bmatrix}^\top, \\ &\omega_c(0,0) = 0.0024 \begin{bmatrix} -1 & 1 & -1 \end{bmatrix}^\top,\ p(0,0) = 0.5 \begin{bmatrix} -1 & \mathbf{1}_3^\top \end{bmatrix}^\top. \end{aligned} \tag{78}$$

The mass of the deputy spacecraft is $m_d = 120$ kg, and that of the chief is $m_c = 360$ kg. The docking points are assumed to be located at the center of one of their faces, and the normal vector is $v = \begin{bmatrix} 0 & 1 & 0 \end{bmatrix}^\top$. During the capture phase, the deputy is controlled as a single rigid body, so we impose tighter actuation bounds of ±1 N in thrust and

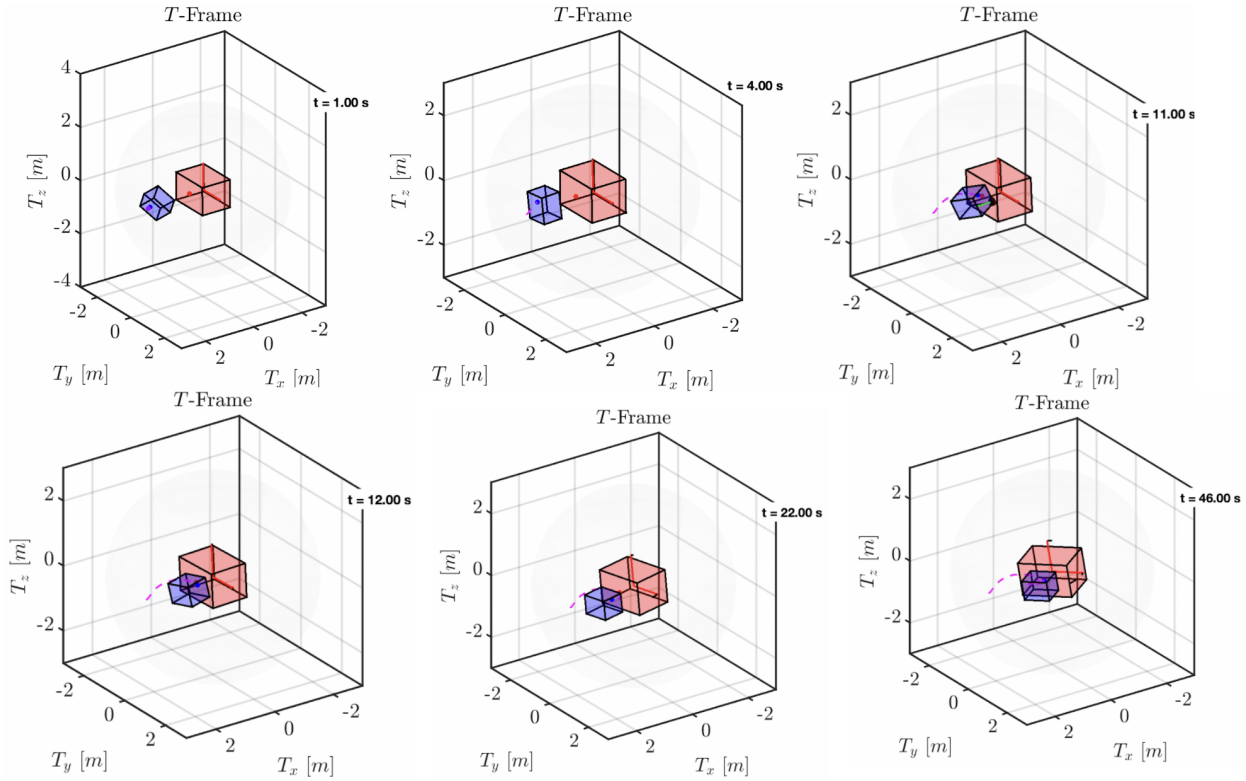

Fig. 5 Capture-phase flow with a contact-induced jump at $t = 11$ s.

±1 N m in torque. After capture, the deputy must regulate the composite chief–deputy motion, which requires greater control authority; thus, the bounds are relaxed to ±5 N and ±5 N m.

The capture-phase objective is to achieve a safe dock in the desired configuration by eliminating relative translation and rotation, i.e., driving the relative position and velocity to zero while simultaneously aligning the deputy attitude with the chief's. To this end, we choose the stage-cost weights $\bar{Q}^0$, $\bar{R}^0$ and terminal cost Q_{f}^0 as in Section VI.A, namely,

$$\bar{Q}^0 = \mathrm{blkdiag}\Big(10^2 I_3,\ 10 I_3,\ 10^3 I_3,\ 10^3 I_3\Big), \quad \bar{R}^0 = \mathrm{blkdiag}\Big(10^4 I_3,\ 10^4 I_3\Big), \quad Q_{\mathrm{f}}^0 = 10^2 I_3. \tag{79}$$

With the initial conditions in (78), the limited capture-phase actuation prevents fully nullifying the relative translation before contact, leading to the first nonresting impact at $t = 11$ s, as shown in Figure 5. Following the collision-induced recovery strategy, the stage and terminal weights are then updated as functions of the collision index c according to

$$\bar{Q}^0(c) = \mathrm{blkdiag}\Big(10^2 I_3,\ 10^{c+1} I_3,\ 10^{c+4} I_6\Big), \quad \bar{R}^0(c) = 10 I_6, \qquad Q_{\mathrm{f}}^0(c) = 10^{c+6}. \tag{80}$$

The prediction horizon is set to $T^0 = 10$ sec). With this short prediction horizon, the optimizer prioritizes correcting the rotational misalignment within approximately one horizon length. All computations were performed on an Apple M3 machine with 16 GB RAM. The optimization problem was formulated using YALMIP [28] and solved using SDPT3 solver [29]. With the constraints (63)–(66) in place, Problem 2 is formulated as a second-order cone program (SOCP). As the prediction horizon increases, the number of decision variables and stage-wise constraints grows proportionally, and the observed solution time (computational complexity for one MPC iteration) in our implementation increases approximately linearly with the horizon length.

Once the rotational states have converged, the optimizer primarily allocates control authority to regulating the translational motion. This trend is reflected in the norm of the commanded actuation input (see Fig. 6), where the torque-related effort becomes negligible after the attitude misalignment is corrected and the remaining control action is dominated by translation. Following a successful docking event, the system transitions to the post–capture phase. The collision contact and subsequent mode transitions are explicitly indicated in Fig. 6.

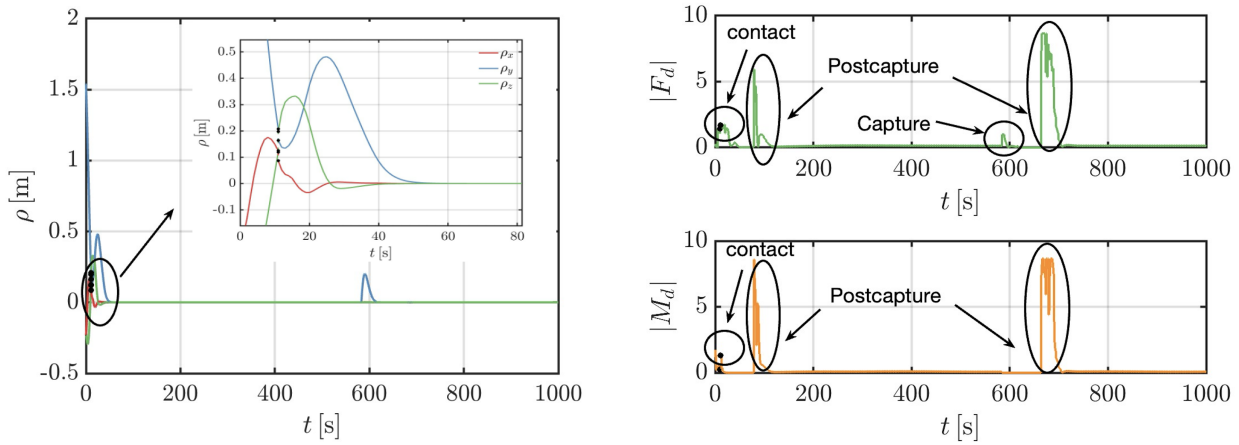

(a) ρ (b) $|u|$

Fig. 6 MPC results: relative displacement between the docking ports and control norms.

After docking, the spring-damper latch mechanism provides additional passive dissipation and further reduces any residual relative motion. The translational and rotational stiffness and damping coefficients in (40)–(42) are chosen as

$$K_T = K_R = 5\, I_3, \qquad D_T = D_R = 2\, I_3. \tag{81}$$

With this spring-damper latch mechanism in place, the relative states remain regulated near zero throughout the post–capture phase. The control objective for the post–capture phase is to damp the coupled tumbling motion of the combined chief–deputy assembly and steer it toward the desired orbital trajectory. In accordance with the post–capture MPC design described in Section VI.B, the weighting matrices are selected to penalize the rotational quantities more strongly than the translational tracking errors, and are chosen as

$$\bar{Q}_1^1 = 10^8 I_6, \quad \bar{Q}_2^1 = 10^4 I_6, \quad , \bar{R}^1 = 10^2 I_6, \quad Q_{\mathrm{f}}^1 = \mathrm{blkdiag}(10^8 I_6, 10^6 I_6). \tag{82}$$

Using these capture and post-capture MPC controllers, as observed from Figs. 6–7, the objectives for both phases are met successfully. During the transition from capture to postcapture, no state resets occur; consequently, ρ, ω, q, p,

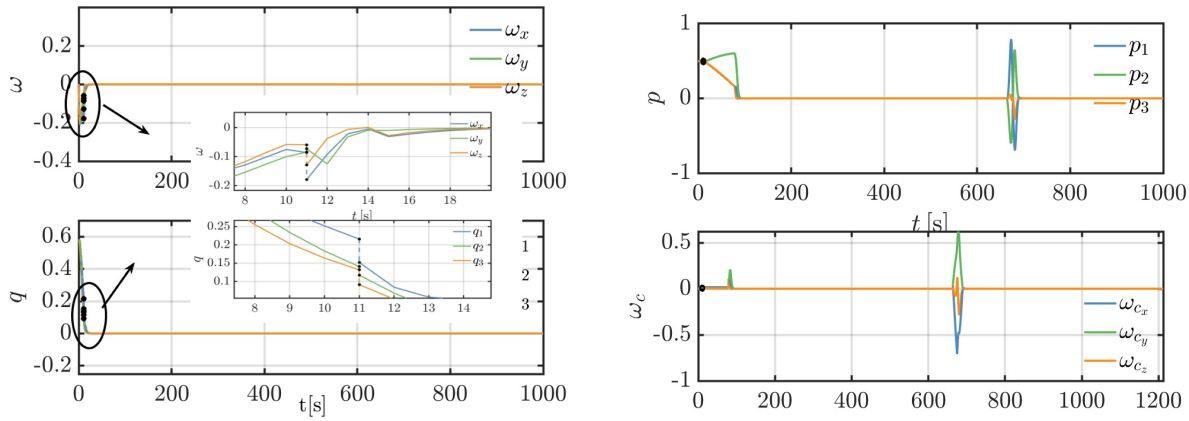

(a) ω and q (b) ω_c and p

Fig. 7 Relative rotational states and angular-velocity and orientation of the chief.

and ω_c in Figs. 6–7 remain continuous (they do not jump) when the controller switches to the postcapture MPC. The

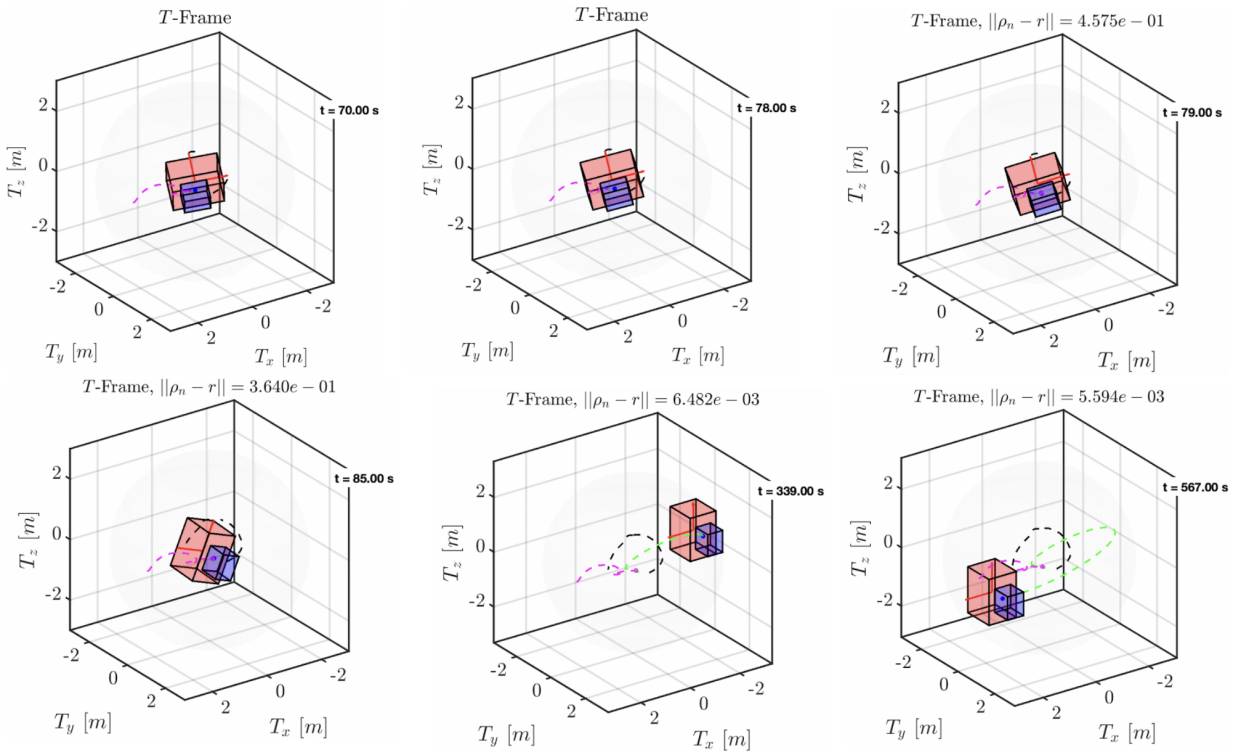

Fig. 8 Postcapture orbital tracking.

relative weighting specified by (82) emphasizes orbit tracking in the postcapture optimization, which can produce small initial transients in p and ω_c, as observed from Figure 7b. Using the postcapture MPC with the weighting matrices in (82), Figure 8 demonstrates a precise orbit tracking with millimeter-level tracking error.

During the postcapture phase, a sudden latch snap may generate an internal impulse of magnitude 0.05N s along the docking interface, applied in the direction of ρ_0, which causes the two spacecraft to separate at approximately $t = 593$s. This loss of contact triggers a reversion to the capture MPC. Because the rotational states are not reset upon decoupling, $|M_d|$ in Figure 6b remains essentially unchanged, whereas $|F_d|$ takes corrective action to regulate the translational dynamics. Once docking is re-established, the controller switches back to postcapture mode and orbit tracking resumes, as shown in Figure 9.

VIII. Conclusion

This paper addresses the rendezvous and docking problem of a chief–deputy rigid-spacecraft system in low-Earth circular orbit with an initially tumbling chief. The proposed framework achieves (i) safe capture and docking in the presence of low-velocity contact events, and (ii) post-capture stabilization of the coupled tumbling motion together with regulation of the composite CoM motion to a prescribed parking-orbit trajectory, while accounting for the possibility of sudden decoupling.

To handle the distinct dynamics, objectives, and discrete events across these stages, we developed phase-specific hybrid models and model predictive controllers for the capture and post-capture phases, and integrated them into a unified hybrid closed-loop architecture. In the capture phase, collision contacts were explicitly modeled and a collision-recovery mechanism was embedded in the MPC design to mitigate contact-induced deviations from the docking configuration. In the post-capture phase, decoupling events were incorporated and the MPC law was designed to simultaneously dissipate residual tumbling while tracking a time-varying orbital reference for the composite system. A hysteresis-based switching logic was introduced to robustly govern transitions between phases and prevent chattering under disturbances.

A numerical case study validated the proposed approach, demonstrating safe docking under tumbling and contact interactions, effective recovery from unanticipated collisions, stabilization of post-capture dynamics, and transfer of the composite system to the desired parking orbit.

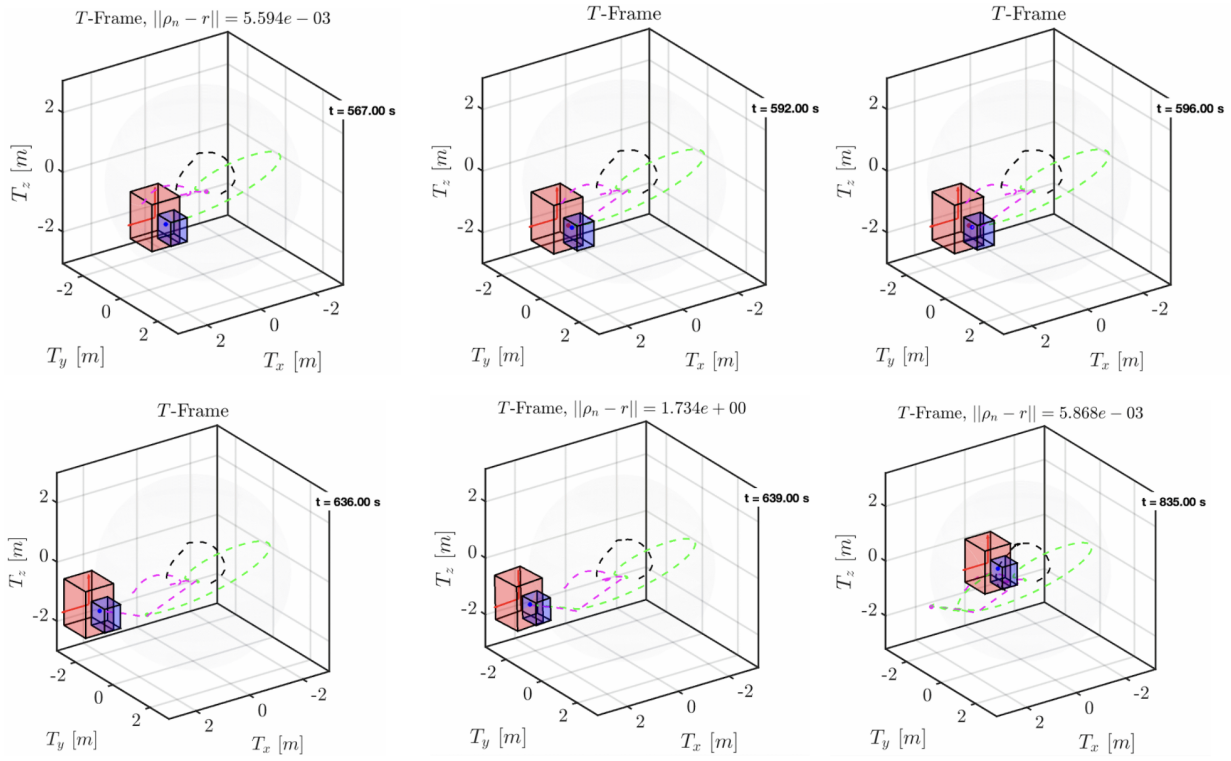

Fig. 9 Decoupling mode, and subsequent transitions between modes.

Acknowledgments

We sincerely acknowledge the support of our funding sponsors. This research was partially supported by NSF Grants Nos. CNS-2039054 and CNS-2111688; AFOSR Grants Nos. FA9550-19-1-0169, FA9550-20-1-0238, FA9550-23-1-0145, FA9550-23-1-0313, FA9550-23-1-0678; AFRL Grants Nos. FA8651-22-1-0017, FA8651-23-1-0004; ARO Grant No. W911NF-20-1-0253; and DoD Grant No. W911NF-23-1-0158.

References

[1] Mote, M. L., Hays, C. W., Collins, A., Feron, E., and Hobbs, K. L., "Natural Motion-based Trajectories for Automatic Spacecraft Collision Avoidance During Proximity Operations," *2021 IEEE Aerospace Conference*, MT, USA, 2021, pp. 1–12. https://doi.org/10.1109/AERO50100.2021.9438434.

[2] Michael, J., Chudej, K., Gerdts, M., and Pannek, J., "Optimal Rendezvous Path Planning to an Uncontrolled Tumbling Target," *IFAC Proceedings Volumes*, Vol. 46, No. 19, 2013, pp. 347–352.

[3] Park, H., Cairano, S. D., and Kolmanovsky, I., "Model Predictive Control for Spacecraft Rendezvous and Docking with a Rotating/Tumbling Platform and for Debris Avoidance," *Proceedings of the 2011 American Control Conference*, CA, USA, 2011, pp. 1922–1927. https://doi.org/10.1109/ACC.2011.5991151.

[4] Cairano, S. D., Park, H., and Kolmanovsky, I., "Model Predictive Control Approach for Guidance of Spacecraft Rendezvous and Proximity Maneuvering," *Int. J. Robust. Nonlinear Control*, Vol. 22, 2012, pp. 1398–1427. https://doi.org/10.1002/rnc.2827.

[5] Malladi, B. P., Sanfelice, R. G., Butcher, E., and Wang, J., "Robust Hybrid Supervisory Control for Rendezvous and Docking of a Spacecraft," *IEEE Conference on Decision and Control (CDC)*, 2016, pp. 3325–3330. https://doi.org/10.1109/CDC.2016.7798769.

[6] Crane, J. R., Roscoe, C. W. T., Malladi, B. P., Zucchini, G., Butcher, E., Sanfelice, R. G., and Hussein, I., "Hybrid Control for Autonomous Spacecraft Rendezvous Proximity Operations and Docking," *IFAC Workshop on Networked & Autonomous Air & Space Systems (NAASS)*, 2018, pp. 94–99.

[7] Weiss, A., Baldwin, M., Erwin, R. S., and Kolmanovsky, I., "Model Predictive Control for Spacecraft Rendezvous and Docking: Strategies for Handling Constraints and Case Studies," *IEEE Transactions on Control Systems Technology*, Vol. 23, No. 4, 2015, pp. 1638–1647. https://doi.org/10.1109/TCST.2014.2379639.

[8] Richards, A., Schouwenaars, T., How, J. P., and Feron, E., "Spacecraft Trajectory Planning with Avoidance Constraints Using Mixed-Integer Linear Programming," *Journal of Guidance, Control, and Dynamics*, Vol. 25, No. 4, 2002, pp. 755–764. https://doi.org/10.2514/2.4943.

[9] Basu, H., Pedari, Y., Almassalkhi, M., and Ossareh, H. R., "Computationally Efficient Collision-Free Trajectory Planning of Satellite Swarms Under Unmodeled Orbital Perturbations," *Journal of Guidance, Control, and Dynamics*, Vol. 46, No. 8, 2023, pp. 1548–1563. https://doi.org/10.2514/1.G007206.

[10] Wu, Y., Cao, X., Xing, Y., Zheng, P., and Zhang, S., "Relative Motion Decoupled Control for Spacecraft Formation with Coupled Translational and Rotational Dynamics," *2009 International Conference on Computer Modeling and Simulation*, Macau, China, 2009, pp. 63–68. https://doi.org/10.1109/ICCMS.2009.12.

[11] Li, Q., Yuan, J., Zhang, B., and Gao, C., "Model Predictive Control for Autonomous Rendezvous and Docking with a Tumbling Target," *Aerospace Science and Technology*, Vol. 69, 2017, pp. 700–711. https://doi.org/10.1016/j.ast.2017.07.022.

[12] Boyarko, G., Yakimenko, O., and Romano, M., "Optimal Rendezvous Trajectories of a Controlled Spacecraft and a Tumbling Object," *Journal of Guidance, Control, and Dynamics*, Vol. 34, No. 4, 2011, pp. 1239–1252. https://doi.org/10.2514/1.47645.

[13] Petersen, C., and Kolmanovsky, I., "Coupled Translational and Rotational Dynamics for Precise Constrained Rendezvous and Docking with Periodic Reference Governors," *proceedings of the* 26^{th} *AAs/AIAA Space Flight Mechanics Meeting*, Vol. 158, 2016, pp. Paper AAS 16–507.

[14] Wu, S., Mou, F., Liu, Q., and Cheng, J., "Contact Dynamics and Control of a Space Robot Capturing a Tumbling Object," *Acta Astronautica*, Vol. 151, 2018, pp. 532–542.

[15] Holland, D., "A Case Study of the Near-Catastrophic Mir–Progress 234 Collision with Emphasis on the Human Factors/Systems-Level Issues Surrounding This Mishap," *INCOSE International Symposium*, Vol. 12, No. 1, 2002, pp. 820–827.

[16] Thomas, L. D., "Selected Systems Engineering Process Deficiencies and Their Consequences," Technical report, National Aeronautics and Space Administration, George C. Marshall Space Flight Center, 2007.

[17] Oberg, J., "Shuttle–Mir's Lessons for the International Space Station," *IEEE Spectrum*, Vol. 35, No. 6, 1998, pp. 28–37.

[18] Basu, H., Castroviejo-Fernandez, M., Sanfelice, R. G., and Kolmanovsky, I., "Hybrid Model Predictive Control Approach for Spacecraft Proximity Maneuvering and Docking Accounting for Collisions," *Proceedings of the American Control Conference*, Denver, CO, USA, 2025, pp. 1–6. URL https://hybrid.soe.ucsc.edu/sites/default/files/preprints/333.pdf.

[19] Jeyakumar, D., and Rao, B. N., "Dynamics of satellite separation system," *Journal of Sound and Vibration*, Vol. 297, No. 1, 2006, pp. 444–455. https://doi.org/10.1016/j.jsv.2006.03.035.

[20] Goebel, R., Sanfelice, R. G., and Teel, A. R., *Hybrid Dynamical Systems: Modeling, Stability, and Robustness*, Princeton University Press, 2012.

[21] Sanfelice, R. G., *Hybrid Feedback Control*, Princeton University Press, New Jersey, 2021.

[22] Mayhew, C. G., Teel, A. R., and Sanfelice, R. G., "Robust Global Asymptotic Attitude Stabilization of a Rigid Body by Quaternion-Based Hybrid Feedback," *IEEE Transactions on Automatic Control*, Vol. 56, No. 11, 2011, pp. 2555–2562. https://doi.org/10.1109/TAC.2011.2159550.

[23] Altın, B., Ojaghi, P., and Sanfelice, R. G., "A Model Predictive Control Framework for Hybrid Dynamical Systems," *IFAC-PapersOnLine*, Vol. 51, No. 20, 2018, pp. 128–133. https://doi.org/10.1016/j.ifacol.2018.11.004, 6th IFAC Conference on Nonlinear Model Predictive Control (NMPC 2018).

[24] Ojaghi, P., Altın, B., and Sanfelice, R. G., "A Model Predictive Control Framework for Asymptotic Stabilization of Discretized Hybrid Dynamical Systems," *2019 IEEE 58th Conference on Decision and Control (CDC)*, Nice, France, 2019, pp. 2356–2361. https://doi.org/10.1109/CDC40024.2019.9029729.

[25] Wang, D., Wu, B., and Poh, E. K., *Satellite Formation Flying*, Vol. 87, Springer, Singapore, 2017. https://doi.org/10.1007/978-981-10-2383-5.

[26] Caccavale, F., Natale, C., Siciliano, B., and Villani, L., "Six-DOF Impedance Control Based on Angle/Axis Representations," *IEEE Transactions on Robotics and Automation*, Vol. 15, No. 2, 1999, pp. 289–300. https://doi.org/10.1109/70.760350.

[27] Bullo, F., and Murray, R. M., "Proportional Derivative (PD) Control on the Euclidean Group," *Proceedings of the 3rd European Control Conference (ECC)*, Rome, Italy, 1995, pp. 1091–1097.

[28] Löfberg, J., "YALMIP : a toolbox for modeling and optimization in MATLAB," *2004 IEEE International Conference on Robotics and Automation*, 2004, pp. 284–289. https://doi.org/10.1109/CACSD.2004.1393890.

[29] Tütüncü, R., Toh, K., and Todd, M., "Solving semidefinite-quadratic-linear programs using SDPT3," *Mathematical Programming, Series B*, Vol. 95, 2003, pp. 189–217. https://doi.org/10.1007/s10107-002-0347-5.